SSRG International Journal of Civil Engineering
ISSN: 2348-8352/ https://doi.org/10.14445/23488352/IJCE-V13I8P117

Volume 13 Issue 8, 255-280, August 2026

Original Article

Sustainable Construction by Utilization of Municipal Solid Waste Incineration - Bottom Ash (MSWIBA) as Material for Developing One-Part 3D Printed Geopolymer Concrete

Prasad Barve[1], Santosh Shah[2], Deep Upadhyaya[3]

[1]*Gujarat Technological University, Ahmedabad, Gujarat, India.*
[2] *Director of Construction, OM Group, Illinois, United States of America.*
[3]*Department of Civil Engineering, Government Engineering College, Godhra, Gujarat, India.*

[2]*Corresponding Authors : drsantoshgshah@gmail.com*

Received: 05 May 2026 Revised: 14 July 2026 Accepted: 20 August 2026 Published: 31 August 2026

Abstract - *The ability of MSWIBA as a precursor for geopolymer mixtures amenable to 3D printing is explored in this research. In geopolymer binders, the MSWIBA is utilized in part substitution of fly ash. Investigations are conducted into how the MSWIBA content affects the fresh qualities of printed formulations, particularly setting time, rheological characteristics, and flowability. Additionally, using different amounts of MSWIBA in the mixture, the hardened characteristics of 3D printable MSWIBA geopolymer concrete are assessed. According to the test findings, the MSWIBA content in the mix has enhanced the fresh characteristics of the optimum 3D printed mix. Excellent early age yield stress and apparent viscosity are demonstrated by the optimum mixture with MSWIBA. The incorporation of MSWIBA up to 10 % has enhanced the compressive strength of 3D printable geopolymer concrete samples, whereas higher MSWIBA concentrations has led to a reduction in hardened properties. Lastly, the suggested one-part geopolymer can lessen the carbon emission and embodied energy by up to 11–38% in comparison with OPC concrete.*

Keywords - *3D printed geopolymer, Mswiba, Rheology, Microstructure, Environmental assessment.*

1. Introduction

Concrete 3D printing has evolved as a transformative technology for the digitalization of the infrastructure sector, owing to its intrinsic benefits of eliminating formwork, minimizing labor needs, improving construction safety, and facilitating architectural creativity for the design of complex structures [1]. Recent research on 3D printed concrete has explored various properties and potential applications, highlighting both advancements and challenges in this emerging field. An investigation explored the usage of steel slag aggregate as a replacement for river sand in 3D-Printed Concrete (3DPC), demonstrating its feasibility through extensive testing of workability, strength, and printability [2]. An optimal mix design and predictive models were developed, offering eco-friendly alternatives for 3DPC applications [2]. Research demonstrated the potential of 3D-printed earth concrete solidified with geopolymer, achieving substantial improvements in strength and reduced porosity while maintaining favorable thermal properties [3]. The results support 3D printed earth concrete as a sustainable solution for low-rise construction with enhanced mechanical performance [3]. Incorporation of Ultra-Fine Glass Powder (UFGP) in 3DPC significantly enhanced its mechanical and hygric properties, as well as thermal resistance [4]. A 20% UFGP replacement yielded optimal performance, with minimal compressive strength loss at elevated temperatures and improved moisture regulation, demonstrating its potential for high-temperature and sustainable construction applications [4]. Researchers introduced a CO_2-activated Interface Enhancer (CIE) using dicalcium silicate to significantly improve interlayer bonding in 3DPC, achieving a 249.3% strength increase at 28 days [5]. The CIE forms an interlocking microstructure through carbonation, offering a promising solution for enhancing print layer cohesion in automated construction [5].

The influence of fiber amount, layer height, and recycled sand replacement on the interfacial properties between 3D-printed ECC and cast concrete were examined in an investigation [6]. Desirable bond strength was obtained at a 15 mm single-filament print height, while full recycled sand replacement significantly reduced interfacial tensile and shear strengths [6]. Predictive models for interfacial shear behavior were also developed [6]. The concrete pumping process in 3D printing significantly influences air content, pore structure, and compressive strength by reducing entrapped air and enhancing hydration kinetics [7]. Inclusion of 0.12% air-entraining chemical reduced the amount of air loss to 23-25%, showing that air entrainment control is necessary to ensure uniform rheology and mechanical attributes [7].

The structural efficacy of 3DPC with automatically placed helical reinforcement was studied, which showed that bond strength, crack spacing and fitting with the conventional analytical models were better [8]. It was found that existing methods are well-suited to 3D printing, but some modifications are necessary for the anchorage and shear detailing [8]. Another research introduced a mesh fabrication in-situ technology for 3DPC, which supported multi-directional reinforcement with epoxy-coated steel fibers and high-flowability epoxy to connect reinforcement segments [9].

The technique also enhanced flexural properties by 123.6%, indicating that it could be used successfully to reinforce 3D printed elements [9]. The anisotropy in mechanical and durability behavior of 3DPC, with compressive and flexural strengths highly dependent on loading orientation relative to print layers was highlighted in a study [10]. Compressive strength up to 85% of cast concrete was obtained when subjected to compression parallel to the layers, and 59% when subjected to compression perpendicular to the layers [10].

The weak zones of interlayer interfaces were found to be vulnerable to moisture penetration and cracking, highlighting the need to consider interlayer bonding and print orientation for structural integrity [10]. Several countries have already implemented concrete 3D printing within the construction sector, resulting in the completion of various large-scale constructions utilizing this technology. Notable instances include an administrative building by Apis Cor in Dubai [11], a concrete bridge in California by the Marine Corps [12], water tanks in Kuwait by Abyan and COBOD [13], a pedestrian bridge erected in China [14] and the first post office in the world, built by L&T and COBOD in India [15].

However, owing to infrastructural growth, rising populations, and quick urbanization, trash production has soared in the last several decades. Worldwide waste produced is predicted to double and triple by 2050 and 2100, respectively, in comparison to 2016 levels, based on a statistical study [16, 17]. Despite global campaigns for recycling waste materials into commodities with additional value, massive amounts of waste are being dumped in landfills. Waste dumping on valuable lands is a serious issue since it threatens human safety and well-being and produces alarming ecological issues, such as the exhaustion of resources and land and the polluting of air, water and soil [16].

Trends are shifting from traditional (non-renewable) resources to renewable ones in this age of sustainable growth to meet the requirements of the general public for energy without having an adverse effect on the environment. Recognizing each country's potential regarding the domain of managing solid waste and then leverage it for the renewable energy industry is a global endeavour. According to the Central Pollution Control Board (CPCB, Delhi, India) report for FY 2022–2023, India generates 1,70,939 Tons Per Day (TPD) of solid municipal waste with a 96% collection efficiency, though per capita generation has risen from 98.79 to 155.87 grams/day over a six-year trend [18]. Comprehensive waste processing infrastructure has expanded significantly to treat 61% (1,04,216 TPD) of total waste, utilizing windrow composting for organic fractions, Refuse-Derived Fuel (RDF)/pelletization for inorganic streams, and 22 operational Waste-to-Energy (WtE) plants generating 207.172 MW [18]. Concurrently, reliance on engineered sanitary landfills dropped to 22% (38,147 TPD), while remediation efforts continue across 2,474 legacy open dumpsites [18].

Consequently, the unaccounted solid waste management gap has been reduced to 17% (28,576 TPD), which was 30.35% in 2018-19, demonstrating systemic improvement in national waste treatment capacities [18]. Based on a report, cities in India are predicted to produce 4,50,132 TPD of waste by 2031 and 11,95,000 TPD by 2050, assuming a 5% yearly increase in the generation of waste [19, 20]. However, in 2020-21, India recorded 49.96% processing and 18.4% landfilling of solid waste in contrast to 19% and 54% in 2015-16, respectively [21]. Food waste, paper, cardboard, glassware, home waste, electronic waste, other waste from places of outdoor activities, metals, synthetic materials, textiles, plastics, and other toxic materials are the main constituents of solid municipal waste in India [22]. The Ministry of Environment, Forest and Climate Change (MoEFCC), enacted the Solid Waste Management Rules (SWMR), 2026, creating a legally binding bridge between municipal waste streams and industrial co-processing while completely barring high-calorific (≥ 1500 kcal/kg) and biodegradable fractions from landfill systems [23]. Waste generators are legally mandated to separate solid waste at the origin into four distinct streams: Dry waste (non-recyclable and recyclable), Wet waste (biodegradable), Sanitary waste (sanitary pads, diapers, etc.), and Special care waste (domestic hazardous waste like expired medicines, paint drums, and bulbs) [23].

The US and other developed nations have acknowledged the potential for waste energy recovery as a sustainable energy source [24]. Developed nations are already using WtE to address a number of waste-related environmental issues [25]. Over 66% of towns in nations like China have currently loaded their landfills to brimming [26]. WtE conversion using municipal solid wastes is becoming more popular for the following reasons: (a) there aren't enough lands available for landfills, and WtE techniques reduce waste volume quickly; (b) they lessen environmental impact; and (c) heat and electricity can be produced from them and offer monetary benefits by recovering useful elements such as recyclable solid wastes, polymers, and metals that can be separated [24, 27-29]. In the last 15 years, India's currently operational capacity of WtE facilities has nearly quadrupled, rising from 43.5 MW in 2007 to 168.64 MW in 2021. Yet only 4.6% of the 3653 MW total capability is now accounted for by the installed municipal solid waste-based electricity production capacity [21]. In order to aid in the upcoming growth of appropriate WtE methods in India, researchers have attempted to address a few open problems [30]. However, the process of burning solid municipal waste produces a critical quantity of by-products, which make up 5–30% of the overall volume of municipal solid waste, comprising of air pollution management residues, bottom ash and fly ash [31, 32]. Landfills are required to dispose of these byproducts, which can be problematic in nations with dense populations and limited area [33]. Furthermore, because harmful leachates can build up in delicate bodies of water, these landfills are likely to endanger the ecosystem if improperly managed [34].

Bottom ash makes about 90% of the total burned municipal solid waste, whereas the remaining is fly ash [35, 36]. The MSWIBA's usage is vital to achieve a circular economy because it makes up a significant amount of the remains of burned solid municipal waste [37]. By incorporating the aforementioned ashes in the construction sector, ecological concerns, waste management expenses, solid waste production, release of gases that cause climate change related to the production of Portland clinker, and the quantity of waste disposal in landfills are all reduced [38]. However, because MSWIBA is rich in aluminosilicates, novel possibilities for it as a geopolymer concrete precursor have surfaced recently as an environmentally friendly substitute to conventional concrete that uses OPC [39, 40]. Alkaline activators are used to activate aluminosilicate materials, along with admixtures and aggregates, to create geopolymer concrete. Fly ash, metakaolin, and Ground Granulated Blast Furnace Slag (GGBS) are among the most extensively researched aluminosilicates for geopolymers [41, 42]. The amalgamation of fly ash and GGBS in geopolymer binders can be used more effectively than using GGBS and fly ash alone because of the synergistic influence between the aluminosilicate-rich fly ash and the calcium-rich GGBS [43]. The binary blending produces a reduction in porosity, an increase in mechanical strength and resistance to thermal and aggressive environmental conditions, since it favors the synthesis of Sodium Aluminosilicate Hydrate (N-A-S-H) type gels in addition to Calcium Aluminosilicate Hydrate (C-A-S-H) type gels [43]. As a result of the diminishing availability of traditional geopolymer precursors, such as fly ash, alternative industry wastes are increasingly needed [44, 45]. The composition of fly ash and MSWIBA are chemically similar [46]. MSWIBA could be utilised as a sustainable strategy for the projected scarcity of fly ash for producing geopolymers. [46].

According to earlier research, MSWIBA offers a lot of potential for producing geopolymers as a precursor [46]. Owing to its irregular shaped particles, alkali-activated MSWIBA mortar presented a greater water demand and a lower slump value in contrast to the class F fly ash alkali-activated mortar developed by researchers previously [47]. Further, in an experimental study, the fresh geopolymer mix containing MSWIBA did not harden for more than 24 hours under room temperature curing [48]. Although the MSWIBA and class F fly ash had a comparable reactivity, it was significantly lesser than that of GGBS [48]. The dissolution behavior of MSWIBA in alkaline environments describes the alkali-activated MSWIBA's slow setting [48]. By applying heating techniques to MSWIBA to encourage the development of reactive crystalline phases, the slow setting issue was resolved and affected the mechanical properties positively affected. The geopolymer paste made with 100% MSWIBA had a final setting time of 52 hours, after MSWIBA was activated using hydrated lime [49]. The fresh mortar mixes were cured at 70℃ or 90℃ to expedite the geopolymerization process in an investigation [47]. The strength in compression of MSWIBA based geopolymer is significantly influenced by the activator's alkalinity. After analyzing strength and dry density indices in non-autoclaved aerated concrete with MSWIBA, calcium carbide slag, and desulfurization gypsum, the optimal mix of MSWIBA content ranged from 60% to 85%, resulting in highest strength in compression of 22.8 MPa at 28 days and a minimum dry density of 600 kg/m^3 [50]. Porosity dropped by 23.49% as the MSWIBA reduced from 90% to 60% in the experimental design [50].

In an investigation [51], the remarkably high-temperature performance (76% compressive strength retention at an exposure of 800 °C), reduced precursor cost by 88%, material cost premium over OPC of only 3.7%, and 66.95% lesser carbon footprint of an optimized alkali-activated GGBS paste containing 6% MSWIBA demonstrated the material's strong potential for sustainable and resource-efficient construction. Mechanically activated MSWIBA from Swedish incineration facilities was shown to be a viable 10–20% substitute for cement in concrete, enhancing workability but diminishing density and compressive strength with higher replacement ratios, while providing a sustainable, environmentally friendly option despite minimal strength improvement from mechanical activation [52]. MSWIBA was effectively valorized into alkali-activated lightweight aggregates by utilizing metallic aluminum as an foaming in-situ agent in a study [53], resulting in ASTM C330-compliant porous aggregates with a strength of 2.8–3.2 MPa and a density of 900–1050 kg/m^3. Lightweight concrete's performance was enhanced (compressive strength up to 37.7 MPa), concrete density was reduced by 8.6-13.9%, and heavy metals were effectively captured below US EPA standards using this procedure [53]. Alkali-activated MSWIBA–GGBS cementitious materials demonstrated a significant MSWIBA replacement threshold (~50%), beneath which increased sodium silicate (Na_2SiO_3) solution dosage augmented compressive strength in a research investigation [54]. Conversely, excessive Na_2SiO_3 (>20%) in high-MSWIBA systems impeded C–A–S–H gel formation and strength progression, offering essential insights for the optimization of waste-based binder design and sustainable MSWIBA application [54]. Results of a review showed that municipal solid waste incineration ashes may replace 50% of concrete aggregate, and it was concluded that geopolymer can stabilize these ashes as a binding agent [55].

Further, in comparison to the above mentioned two-part geopolymers, which are prepared from activators in a liquid state, the one-part geopolymers prepared by making use of activators in powder form offer a greater advantage in terms of easy handling, storage and transportation of solid activators in contrast to viscous and corrosive liquid activators [56]. Moreover, the prepared one-part geopolymer proves to be economical and suitable for large-scale and commercial applications since a small amount of solid activator in powder form is required relative to a large quantity of liquid activators [57]. In an experimental investigation [58], a one-part geopolymer concrete activated with 14% anhydrous sodium metasilicate, utilizing a GGBS–fly ash proportion of 60:40, attained a compressive strength 15–20% superior to that of OPC concrete, with just a minor decrease (~3%) in split tensile strength, indicating its viability as a high-strength, low-carbon, and practical substitute for traditional two-part geopolymer and OPC concretes.

One-part geopolymer ambient-cured concrete using GGBS, fly ash and up to 30% waste foundry sand achieved optimum performance with a balanced 50FA–50GGBFS binder (47.15 MPa compressive strength, <3% water absorption, and <2% chloride-induced mass loss), while matrix densification through co-occurring N–A–S–H and C–A–S–H gels, elimination of liquid alkali activators, and complete cement replacement underscore its capability as a circular, low-carbon and resource-efficient construction material [59]. A multiscale experimental-computational study [60] revealed that extending printing intervals in one-part 3D-printed geopolymer concrete exacerbated anisotropy by enhancing pore growth (up to 47.2%), pore elongation, and stress concentration. A validated pore deformation model and finite element analysis corroborated that keeping printing intervals under 0.5 hours is essential for maintaining interfacial bonding and mechanical integrity [60]. A high aggregate-to-binder ratio (1.9) allowed the researchers in the development of 3D printed one-part geopolymer concrete with balanced printability, containing GGBS and fly ash, where fly ash replacement with metakaolin improved rheological performance and buildability but reduced compressive strength (by up to 34.9% at full replacement) while forming C-(N)-A-S-H and C-A-S-H gels that densified the matrix [61]. The developed geopolymer exhibited satisfactory tensile and fracture properties, rapid early-age strength development (62–78% of 28-day strength by 7 days), negligible post-28-day strength gain, and consistent compressive strength irrespective of aggregate moisture condition or curing regime [62].

Although a few researchers [63-65] have attempted to investigate the properties MSWIBA based one-part geopolymer using solid activators, the literature available is scarce. Moreover, the limited literature [66] is available on the rheology of MSWIBA-based formulations. Owing to the heterogeneous behavior of the material in MSWIBA and the presence of reactive contaminants like metallic aluminium and soluble salts, the rheological properties of geopolymers based on MSWIBA have not been fully investigated [67, 68]. Existing studies on MSWIBA-based geopolymer have focused on mechanical properties, with only a few studies including a characterization of the rheology, especially for one-part systems and 3D printing [68, 69]. The study of 3D printing geopolymer concrete is still in its growth phase, and the use of unconventional precursors like MSWIBA is a fairly new field [68]. To achieve 3D printed structures having high-performance, printable concrete's rheological qualities are crucial [70].

Hence, the rheological features [71] such as viscosity, thixotropy and yield stress are important to be explored for successful 3D printing of MSWIBA-based one-part geopolymers. Nonetheless, it has to be investigated whether the resultant thixotropy and yield stress is adequate to augment the buildability of optimum 3D printable MSWIBA-based one-part geopolymers. In addition, since the 3D printed objects are layered structures, they exhibit inherent anisotropic behavior related to the evaluation of mechanical properties [72]. A thorough review of the use of 3D printing in geopolymer concrete, including print techniques, the characteristics of fresh and cured 3D printed geopolymer concrete, and the prospective advantages of construction 3D printing, is available in other sources [73, 74].

The viability of employing MSWIBA as the precursor to the cutting-edge construction technique of concrete 3D printing is examined in the present research. Different ratios of MSWIBA were used to make four different geopolymer concrete compositions that could be 3D printed. The optimum 3D printable mixture's rheological characteristics, encompassing viscosity and static yield stress, were examined. Additionally, the hardened characteristics, such as strength in compression in three orientations and density, were assessed and contrasted with the 3D-printed geopolymer not containing MSWIBA. Furthermore, the microstructural characteristics was assessed. Ultimately, the energy usage and CO_2 emissions of the formulated 3D printed MSWIBA geopolymer optimum mixture were quantified and juxtaposed with those of the conventional 3D printable OPC mix.

1.1. Research Significance

To bridge the existing gaps in sustainable digital construction binders, the primary focus of this research is to formulate and characterize a novel one-part 3D printable geopolymer concrete utilizing MSWIBA as a partial precursor. This work's uniqueness is found in its transition from conventional, corrosive two-part liquid-activated systems to an operationally safer, dry-powder activated one-part geopolymer, uniquely tailored to overcome the rheological complexities of highly heterogeneous municipal waste. By systematically mapping the effect of MSWIBA on thixotropy, viscosity recovery, and yield stress, this research advances the field by achieving high structural buildability (demonstrated via a 600 mm tall printed element). Furthermore, this study originalizes the assessment of this specific composite by quantifying its inherent anisotropic mechanical behavior and substantiating its ecological viability through a direct comparative analysis of embodied energy and carbon emissions against traditional OPC-based 3D printing mixtures.

2. Methodology

2.1. Materials

The commercially available Pozzocrete® 60 fly ash, manufactured by Dirk India in India, GGBS and MSWIBA are utilized in varying amounts as silicoaluminate precursors to formulate the one-part geopolymer binder. Confirming to IS 3812 (Part-1):2013, the fly ash was procured from a local supplier and possesses a fineness – specific surface of 340 m^2/kg, lime reactivity (min.) of 5.48 N/mm^2, moisture content (max.) of 0.27%, autoclave expansion (max.) of 0.029%, and loss on ignition (max.) of 1.6. The GGBS confirmed with IS 16715:2018, with slag activity index greater than 105 at 28 days, as given by the supplier.

The MSWIBA was sourced from Abellon Clean Energy Limited at its 7.5 MW Goodwatts WtE plant located in Jamnagar, Gujarat, India. The plant's MSWIBA was heterogeneous; thus, it needed to be milled before it could be utilized as a starting point for the formulation of the geopolymer binder. Manual removal of any plastic, wood or metal fragments was performed priorly and the MSWIBA was oven-dried for 24 h at 105°C to remove residual moisture. For grinding purposes, the dried material was immediately placed into a Los Angeles abrasion testing machine for 1 h with 21.36 kg of steel balls that were 48 mm in diameter. After passing through a 75 μm standard sieve, the output powder material was utilized as a precursor for the formulation of a one-part geopolymer. A similar procedure for sample preparation of MSWIBA was employed by researchers previously [34]. It should be noted that no extra care was taken to refine the MSWIBA, and the 1 h grinding process was not prolonged, in order to more accurately replicate practical field conditions in the future. Furthermore, additional steel balls of varying sizes and longer milling times are needed to reduce the grain size of MSWIBA, which can be more expensive, time-intensive, and less energy-efficient. The fine aggregates comprised of silica sand in the preparation of the geopolymer. Sodium metasilicate (Na_2SiO_3) anhydrous (Na_2O/SiO_2 = 1:0.9371, as given by the supplier) procured from Associated Finechem Pvt. Ltd., Gujarat, India, was used in powder form as a sole one-part activator for this study. Furthermore, to extend the one-part geopolymers' open time, sucrose powder was added as a retarder [75, 76].

The particle size grading curves for GGBS, fly ash, sand and MSWIBA, as found using a laser diffraction particle size analyzer having a particle size range from 0.1 μm to 875 μm, whereas Malvern Panalytical Mastersizer - v3.88 was used for fine sand, are shown in Figure 1. The physical properties of binders are listed in Table 1. It is evident that fly ash and MSWIBA have nearly identical fineness, nevertheless longer milling durations can remove the small difference.

The chemical composition of fly ash, GGBS, and MSWIBA is displayed in Table 2, as measured by the X-Ray Fluorescence (XRF) Spectrometer. The XRF results revealed that MSWIBA could function as an aluminosilicate precursor for geopolymer since it included significant amounts of SiO_2 and Al_2O_3, two oxides that are essential for geopolymerization reactions.

The Field Emission Scanning Electron Microscopy (FESEM) images of fly ash, GGBS and MSWIBA are shown in Figure 2. The images reveal the morphology of the precursors used to synthesize the one-part geopolymer mixtures. The fly ash particles are spherical, while GGBS particles appear angular in shape. Owing to the grinding process, the shape of the MSWIBA particles appears angular and irregular, as seen in the SEM images. Similar microstructure of MSWIBA was reported in an earlier study [47].

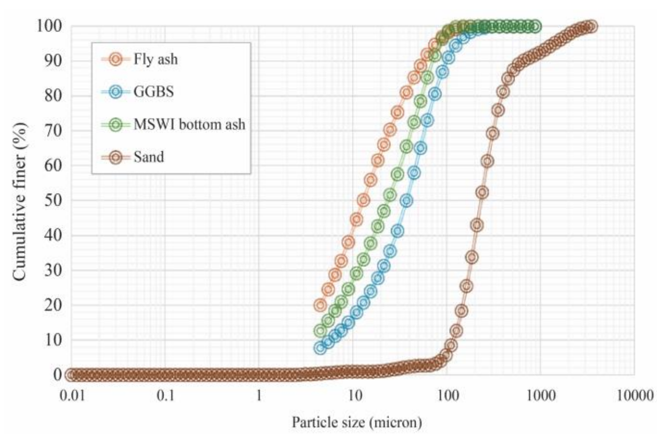

Fig. 1 Particle size distributions of fly ash, GGBS, MSWIBA and sand

Table 1. Physical properties of fly ash, GGBS and MSWIBA

Property	Fly ash	GGBS	MSWIBA
D50 (median particle size, μm)	12.98	37.56	23.79
D90 (μm)	56.75	101.17	71.65
Specific gravity	2.3	2.86	2.17

Table 2. Oxide (%) compositions of the precursors found by XRF

Element	Fly ash (%)	GGBS (%)	MSWIBA (%)
SiO_2	60.667	39.379	37.935
CaO	1.504	23.114	15.476
Al_2O_3	28.759	19.636	11.828
Fe_2O_3	4.844	0.615	8.626
K_2O	0.53	0.468	1.510
MgO	0.901	11.003	6.808
Na_2O	0.555	1.543	7.312
SO_3	0.387	3.450	5.400
TiO_2	1.071	0.374	1.046
P_2O_5	0.381	0.013	2.510
MnO	0.132	0.098	0.214
Cr_2O_3	0.039	0.040	0.099
Rb_2O	0.008	0.005	0.007
SrO	0.028	0.079	0.108
Y_2O_3	0.010	0.009	0.004
ZrO_2	0.059	0.057	0.050
BaO	0.047	0.117	0.162
PbO	0.012	-	0.089
ZnO	0.023	-	0.484
CuO	0.010	-	0.238
Nb_2O_5	0.006	-	0.003
NiO	0.011	-	0.060
Ga_2O_3	0.009	-	-
Co_3O_4	0.007	-	-
CdO	-	-	0.015
Sb_2O_3	-	-	0.017

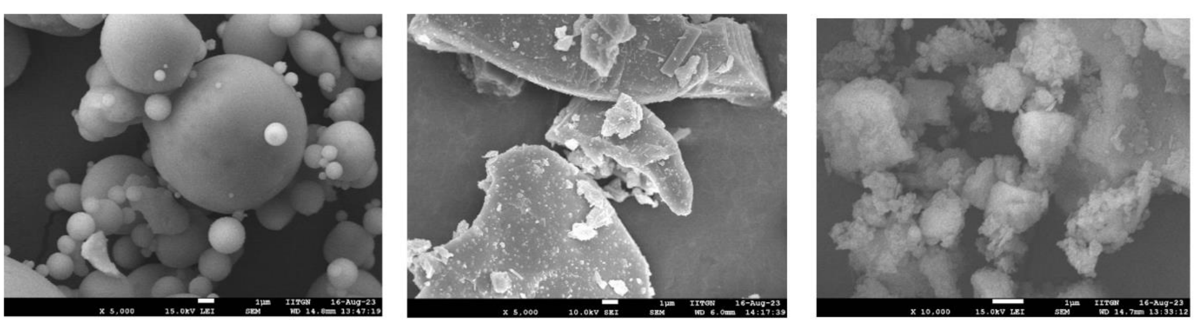

(a) (b) (c)

Fig. 2 FESEM images of (a) Fly ash, (b) GGBS and (c) MSWIBA.

2.2. Sample Preparation

The mix quantities of the ingredients utilized for developing various kinds of one-part geopolymers that are 3D printable are listed in Table 3. As a part substitute for fly ash, the MSWIBA was added to the MSWI-1, MSWI-2, and MSWI-3 mixes at proportions of 10%, 30%, and 50% of the precursor, respectively. Here, all the mixes had the same amount of precursor. Furthermore, a consistent mass ratio of 1.5 was maintained between the total sand and the precursor components. All of the formulations were activated using a

10% precursor weight sodium metasilicate anhydrous (Na_2SiO_3) powder activator. According to earlier studies, this is the optimal amount of powder activator for synthesizing one-part geopolymer [56, 77]. It should be highlighted that, for examining the impact of adding MSWIBA to the 3D printing one-part geopolymer concrete, the GGBS, sand, water and solid activator of all the mixes were kept the same except for the precursor ingredients (fly ash and MSWIBA).

The mixing procedure was performed in 3 steps in a Hobart mixer as follows: Firstly, the components were mixed dry at low speed for 2 minutes, except GGBS. Then add 85% of the total water and continued mixing at medium speed for another 10 minutes. Lastly, GGBS was added and continued mixing at high speed while slowly adding the remaining amount of water to achieve a homogenous mix. The remaining water prevents the mix from losing workability as a result of the powder activator dissolution, as has been documented in earlier research [76]. This is primarily to ascertain that the powder activator dissolves completely during the mixing procedure [76]. The purpose of not adding GGBS at the beginning is that since GGBS is highly reactive as compared to fly ash, it may take up most of the silicate, leaving too little for fly ash to react with, resulting in an undesirable geopolymer product [78].

Table 3. Mixture combinations of one-part 3D printed geopolymer

Mixture ID	GGBS (g)	Fly ash (g)	MSWIBA (g)	Water (g)	Sodium metasilicate anhydrous powder (g)	Sand (g)	Sucrose powder (% of precursor)
MSWI-0	200	200	-	140	40	600	1.0
MSWI-1	200	160	40	140	40	600	1.0
MSWI-2	200	80	120	140	40	600	1.0
MSWI-3	200	-	200	140	40	600	1.0

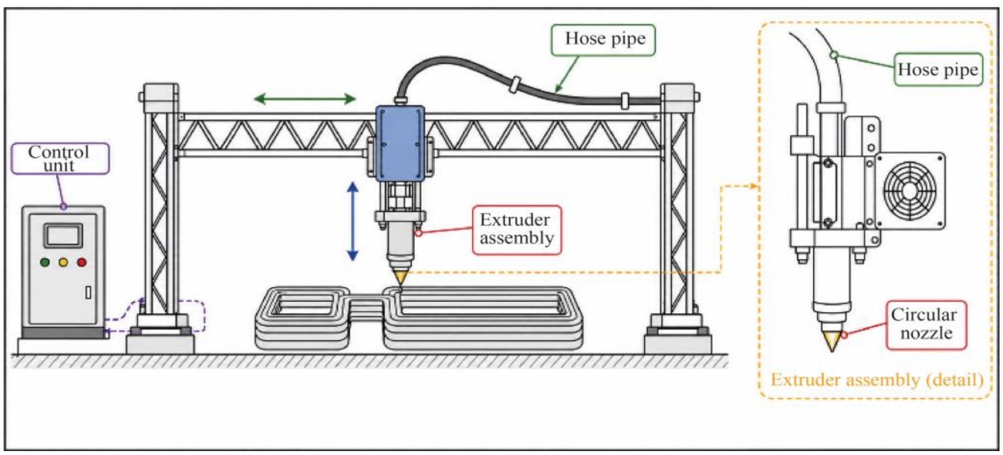

Fig. 3 Gantry-based concrete 3D printer employed for current research

2.3. Procedure for 3D Printing

The geopolymer samples were printed using a concrete 3D printer of the three-axis gantry type, as shown in Figure 3. A homogenous mix is priorly prepared in a pan mixer, which is poured into a hopper. The fresh mix from the hopper is pumped using a progressive cavity pump, which travels through the 5 m long hose pipe (50 mm diameter) and reaches the extruder having a motor-driven auger. The mix is then extruded out from the 30 mm diameter circular nozzle. The printing capacity of the printer is 10 m (W) × 5 m (H) with the length as required. The extruder operated through a specifically built software application within the machine's program interface. The speed was kept 90 mm/s for printing. For the mechanical tests, geopolymer slabs were printed measuring 350 mm x 180 mm x 140 mm. Each filament was print with the following dimensions: 350 mm (L), 30 mm (W), and 20 mm (H). Each layer had 6 adjacent filaments. The slab consisted of 7 printed layers in an S-shape pattern [56]. The time elapsed in printing each layer was about 80 s. The printed specimens were left as it is on the printing platform in the laboratory till the date of testing. Temperature and humidity conditions while printing and curing were 27 ± 2℃ and 65 ± 5%, respectively. Furthermore, to compare the attributes with printed samples, 50 × 50 × 50 mm^3 cubes were also cast.

3. Experimental Planning

3.1. Fresh State Characteristics

3.1.1. Flow Assessment of Fresh Mixture

Pumpability and buildability are the two key opposing needs for the concrete mixtures that can be 3D printed, and they are connected to the fresh characteristics [79]. Slump flow assessment is associated to the pumpability and dynamic yield stress of the 3D printed mixes, whereas fresh mixture's slump measurement aids to assess the buildability and static

[80]. Thus, in accordance with IS 5512:1983, a flow table apparatus was employed to measure the flow measurements of the fresh mixes. While performing the flow table test according to IS 4031 (Part 7):1988, care was taken that the mould of the apparatus was taken away from the mixture one minute following the end of mixing and then instantly drop the table 25 times in 15 s. This controlled timeframe was rigorously upheld during every test to ascertain consistency and minimize the influence of time-dependent rheological changes.

3.1.2. Rheological features

To assess the rheological features of fresh mix, the Schleibinger Gerate eBT2 concrete rheometer was employed, as shown in Figure 4. A vane probe with a six-blade was used to take the measurements by operating the rheometer in the V-mode. Each blade had a radius = 51.5 mm and a height = 103 mm. The container used to fill it with fresh concrete had a radius of 129 mm. The rotation speed limit of the rheometer was 40 rpm. Approximately 40 litres of the sample volume is required to fill the container up to the upper edge, such that the probe gets completely immersed in it. Care was taken that the lower surface of the rheometer does not come in contact with the fresh mix. The placement of the wings in a star pattern nearly eliminates sliding on the probe's wall. The device holder with built-in anti-slip rods also prevents wall slippage on the surface of the container. On the device holder, the eBT2 is fixed, and on the driving shaft, the vane probe is fastened. The torque applied to the rotating vane probe is recorded. It should be noted that during the rotation for taking the measurements, there was no slip between the vane probe and the drive shaft. The speed profile was freely programmable and was input in the smartphone, which is connected to the rheometer via Bluetooth. After completion of the experiment, the rheometer sends the measurement data to the smartphone, which are transferred to the computer for post-processing.

Fig. 4 Rheometer setup employed to assess the rheological characteristics of fresh MSWI-1 mix

The process of concrete 3D printing typically entails an initial phase of high shear during blending of ingredients, succeeded by low shear during pumping, and subsequently high shear during extruding and finally the placing of layers. The apparent viscosity decreases markedly from a greater to a lower reading as the shear rate transitions from low to high, in concrete and other shear-thinning materials [81]. It is essential to verify that the material regains its apparent viscosity after experiencing a high shearing action and a subsequent low shearing. An apparent viscosity recovery test is typically conducted to evaluate this phenomenon. Fresh mortar's apparent viscosity recovery was assessed following the methodology outlined in [17]. Figure 5 (a) depicts the shearing protocol employed for measuring viscosity recovery. For determining the rate of recovery, the values of apparent viscosity were assessed in three steps as illustrated in Figure 5 (a). To mimic the behavior during the rest period prior to printing, the mixture was subjected to shear for 60 s at a steady 5 rpm in the 1st step. To replicate the extrusion or printing process, a peak shear rate of 35 rpm for 30 s was employed for the mixture in the 2nd step. In order to depict the mixture's form retention behavior [81], the mix was finally sheared at a rate of 5 rpm for 60 s to imitate its placement following extrusion in the 3rd step.

After the mix is placed inside the container, a hysteresis test [82] was conducted at a speed raising from 5 rpm to 35 rpm in 60 s, followed by 60 s of steady speed, and further decreased to 5 rpm in 60 s, as illustrated in Figure 5 (b). To rotate the vane probe at first (when the material is at rest), a greater torque is needed, and the torque pick value is compared to the static torque. The material's thixotropy is the cause of the variation between the dynamic and static stresses. The shear stress and plastic viscosity was estimated using the Bingham model [83] for non- Newtonian fluids.

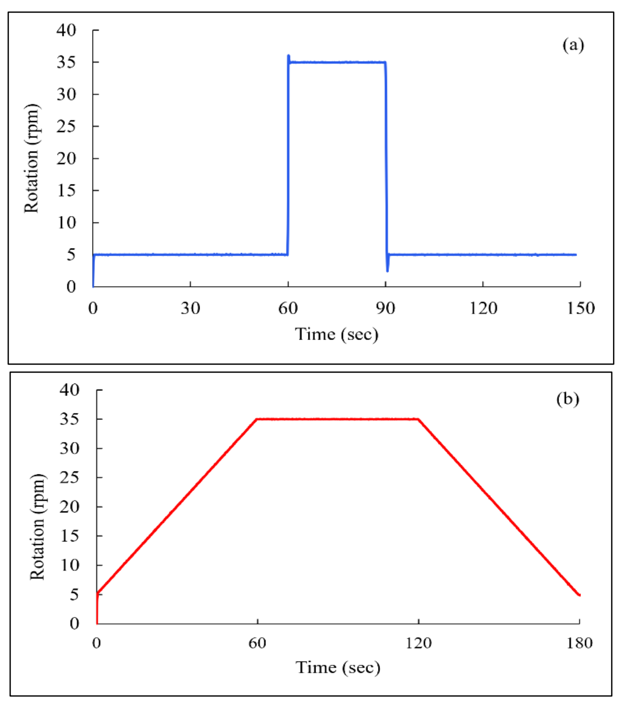

Fig. 5 Rheology test protocols for (a) Viscosity recovery test and (b) hysteresis test.

3.1.3. Setting Time Determination

The rate of reaction with the incorporation of MSWIBA in 3D printable mixtures was evaluated by determining the setting times of fresh geopolymer compositions. The Vicat needle apparatus was employed to ascertain the fresh pastes' (without sand) initial and final setting time as per IS 4031 (Part-5):1988.

3.2. Hardened State Characteristics

3.2.1. Compressive Strength Assessment

The strength in compression of cylindrical cores obtained from 3D printed slabs was measured, and the corresponding cube strengths were calculated in three orientations: perpendicular, lateral, and longitudinal, to study the nature of anisotropy of the specimens that were 3D print. The diagrammatic representation of samples taken from printed slabs and their compressive strength test orientations is displayed in Figure 6. The examination was performed on cylindrical cores measuring height = 130 mm and diameter = 65 mm (height/diameter = 2) at 28 days of age. A 3000 kN load capacity compression testing machine (complying with IS 14858: 2000) was operated at the loading rate of 0.583 kN/s as per IS 516 (Part 1/Sec 1): 2021. For testing in every direction, three specific specimens were used, and their average was considered. Furthermore, a comparison was conducted between the strength in compression of the mold cast samples after 28 days and that of the 3D printed samples, utilizing 50 × 50 × 50 mm^3 mold cast cubes tested under identical loading rates.

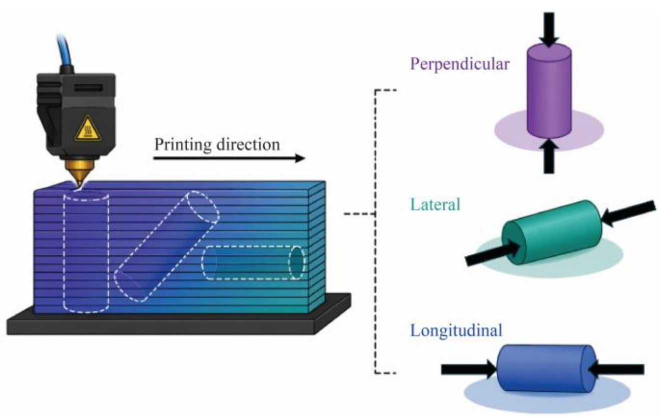

Fig. 6 Diagrammatic representation of samples taken from printed slabs and their compressive strength testing orientations

3.2.2. Density Measurements

The bulk densities of the cast and print specimens were determined by averaging the measurements from three samples after 28 days curing period at ambient conditions.

3.3. Microstructure Characterization

Prior to testing, the samples underwent gold sputtering and were subjected to FESEM on a JEOL JSM 7600 F electron microscope (accelerating voltage = 10-15 kV) to examine the precursors' morphology.

4. Results and Discussion

4.1. Fresh State Characteristics

4.1.1. Flow and Setting Time

The testing outcomes of the slump-flow experiment for formulated mixtures, both prior to and following the dropping of the flow table, are presented in Figure 7. It also includes the setting time as determined by the penetration test using the Vicat needle apparatus. Excellent shape retention, along with favorable pumpability characteristics, were seen in the test results when the geopolymer precursor was partially replaced with MSWIBA.

The control mix designated as MSWI-0 was selected depending on the optimal 3D printable geopolymer concrete formulation, characterized by its no-slump specifications. The mixture MSWI-0 had a flow diameter of 100 mm recorded prior to table drop, which indicates no slump because no flow was seen when the cone was raised.

In addition, without adjusting the water-to-binder ratio, all other mixes containing MSWIBA exhibited a 100 mm diameter spread prior to the table dropping, indicating that there was zero slump in these mixtures. This indicates that all mixtures must demonstrate superior shape retention characteristics, irrespective of the MSWIBA proportion in the geopolymer mixture.

The slump-flow diameter variation is represented by the slump-flow observations made by 25 drops of the flow table. Figure 7 illustrates how the fresh mix's flowability has been negatively impacted by the rise in MSWIBA content, as the mixes' flow diameters have decreased. MSWI-1, MSWI-2, and MSWI-3 flow diameters were 3.2%, 7.7%, and 11.5% smaller than the control mix (MSWI-0).

This may be because irregularly shaped MSWIBA particles replaced the round and spherical fly ash particles, which eliminated the ball-bearing action. Additionally, because MSWIBA powder has a high capacity to absorb water, the flowability drops as the quantity of MSWIBA in the composition rises.

In contrast, when the MSWIBA content increases, so does the fresh mix's setting time. This is mostly because, in comparison to the fly ash precursor, the MSWIBA precursor has a lower geopolymerization reaction rate. The MSWI-1, MSWI-2, and MSWI-3 mixes had slightly longer initial and final setting times (12–38 min) than the MSWI-0 mixture, as indicated in Figure 7.

The printed object's buildability is not anticipated to be substantially impacted by such an increase in setting time. Similar observations regarding the influence of MSWIBA on the setting times and flowability has been reported by researchers [47, 48, 63] in the literature.

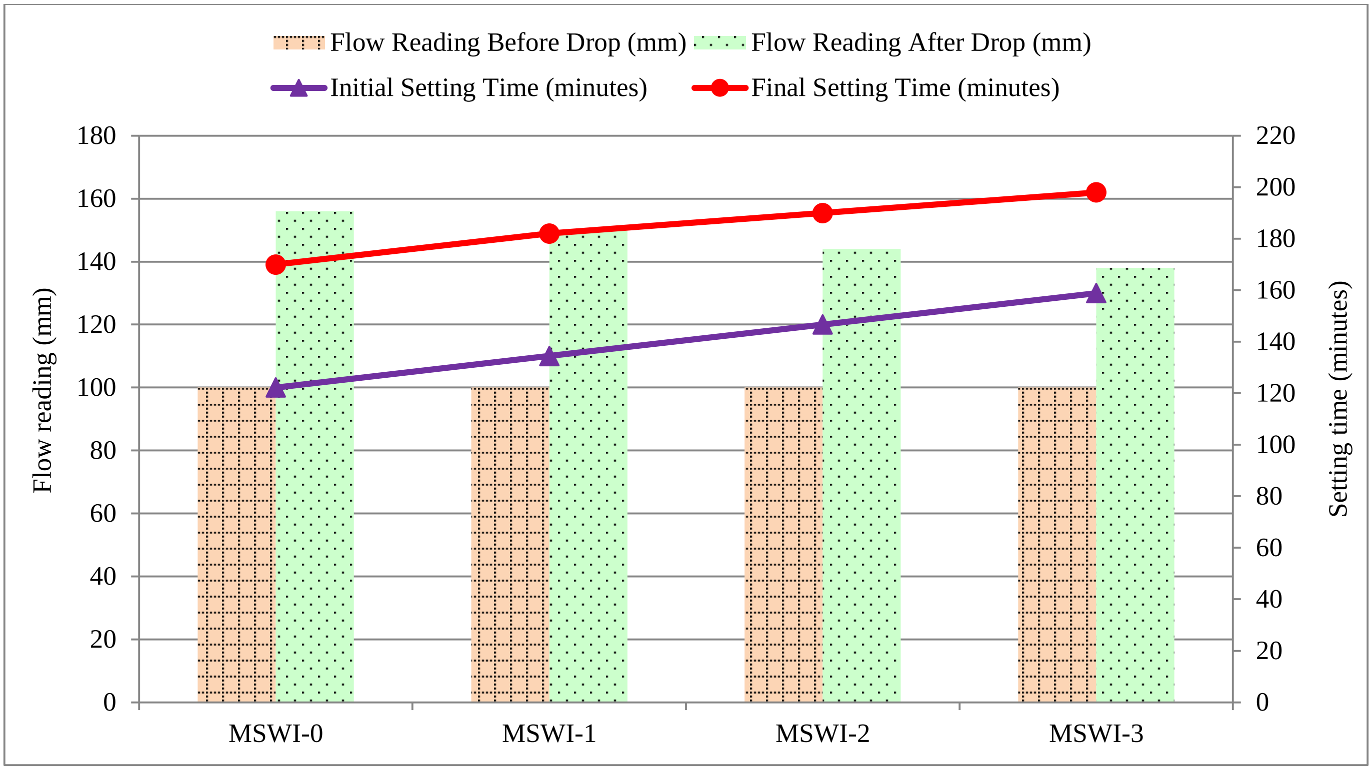

Fig.7 Slump flow and setting time readings of 3D printable mixtures in fresh state

4.1.2. Printability and Rheological Properties

Based on the slump-flow and setting time experiment findings, the 3D printability assessment related to pumpability, extrudability, shape retention and buildability was conducted, and consequently the rheological properties were determined for the optimum mix with desirable printability.

The pumpability assessment for the MSWI-2 composition is revealed in Figure 8 (a). Discontinuous extrusion was observed from the pump outlet (Figure 8 (a)), and the extruded material appeared to have lower fluidity and substantial air entrapment. Based on past experience, this shall lead to the choking of the hose line. Looking to the unacceptable pumpability, the mix MSWI-2 was discarded for further printability and rheology analysis. Further, the mix MSWI-3 was unacceptable for printability assessment, since it was unable to pump it out from the pump outlet. This is in line with the observations and results of the slump-flow test. The mix MSWI-1 exhibited smooth and continuous extrusion from the pump outlet prior to the hose pipe attachment. Further, the hose line is connected to the extruder assembly at one end and the pump outlet at the other. Continuous extrusion of the MSWI-1 mixture was achieved by pumping it via the hose pipe (Figure 8 (b)), exhibiting negligible air entrapment. If there is air entrapped while pumping, it may lead to discontinuity while printing. Thus, the formulated one-part geopolymer mixture MSWI-1 exhibited satisfactory pumpability and extrudability.

The shape retention and buildability were assessed for the mix MSWI-1 through the printing of a cylindrical structure, as displayed in Figure 8 (c). The optimum mix MSWI-1 was prepared to 3D print employing a gantry-type 3D printer. About 30 successive layers have been print consistently and uninterrupted at a height of 600 mm of the printed structure; no discontinuities were noticed between the prints. Thus, it refers to recycling waste in construction applications and confirms the MSWIBA’s potential for concrete 3D printing [84].

Rheometers were employed in the majority of the past investigations to quantify the plastic viscosity and dynamic yield stress [85]. Results may differ greatly because rheometer measurements are susceptible to protocols and are under the rheologists' control [86]. Additionally, if non-standardized measuring geometries are employed, data processing may also affect the measurement output [86, 87]. It takes time and effort to interpret rheological readings, and rheometers may not be available, especially on field where it is critical to determine the printability of mixtures just prior to printing [86]. As a result, such parameters are inappropriate to apply to every batch of concrete mix so as to only give a reasonable evaluation of whether the mixture can be printed to ensure the structure's quality [88]. Scientists in the past have proposed standardized site-friendly procedures based on slump and slump flow experiments [89] to gauge the printability range of concrete mixes for applications in 3D printing [80, 88]. They attempted to predict whether the concrete mix is appropriate for 3D printing employing slump and slump flow measurements [90]. Using the simplified approach, the findings aid to confirm the printability of the mixes prior to 3D printing [80]. This will make the task of developing materials for printing easier in the future, accompanied by saving material, resources and time [91]. The slump flow values (Figure 7) of MSWI-1 mix appear in line with the slump flow findings of the 3D printable mix available in the literature [17, 80]. Thus, the MSWI-1 mix can be considered to be the optimum 3D printable MSWIBA-based one-part geopolymer concrete mix determined by the slump-flow and printability assessment. To support and correlate with these findings, the authors have performed rheometer testing and microstructural characterization for the optimum printable mix MSWI-1.

Fig. 8 Printability assessment of (a) Mix MSWI-2, (b) Mix MSWI-1, and (c) 3D printed structure using MSWI-1 mix.

Rheological properties of fresh geopolymer mixtures are key to its 3D printability, especially its buildability, or the capability of the printed mix to hold up successive filaments resisting collapse or distortion [92]. Apparent viscosity recovery and yield stress are important parameters for the ability of a mixed to transform from a pumping condition to a structurally stable state after deposition, among various rheological conditions [93].

The observed good recovery of apparent viscosity properties for the experimental mixes could guarantee the possible use of MSWIBA as a precursor of a 3D printable geopolymer concrete mixture. Under the shearing conditions proposed, a mixture which can be printed will show a greater recovery to its initial apparent viscosity, thus demonstrating an excellent viscosity recovery behavior. Figure 9 (a) illustrates the apparent viscosity for the MSWI-1 composition at the described shearing protocol. The apparent viscosity measurement is split into three steps here; step 1 refers to the resting time prior to extrusion, with high apparent viscosity recorded. Step 2 is the flowable but lower apparent viscosity state, where the material is at the point of being extruded, and step 3 is high viscosity (viscous flow), where the material is deposited and where it must stay in place once it has been extruded. The MSWI-1 mix exhibits superior apparent viscosity recovery behavior, as seen in Figure 9 (a). This indicates that the re-flocculation ability of MSWIBA is better, providing better buildability properties while printing. In addition, the apparent viscosity increases with the addition of MSWIBA, as evident from the apparent viscosity in step 3. This is an important behaviour to keep complex geometries intact during 3D printing, especially if printing tall or slender elements without formwork [94].

To gain a better understanding of the fresh MSWI-1 mix's structural breakdown and rebuilding properties, a hysteresis loop test was undertaken. As observed in Figure 9 (b), the test involved a controlled ramp-up of rotational speed to 35 rpm from 5 rpm over 60 seconds, a steady state at 35 rpm for 60 seconds, and a subsequent ramp-down to 5 rpm over the next 60 seconds. The growth of shear stress for MSWI-1 mix with shear speed is displayed in Figure 9 (b). The shear stress vs. rotational speed curve shows a typical hysteresis loop, a direct indicator of thixotropic behavior. As shown in Figure 9 (b), the MSWI-1 mix has a high static yield stress of 1580.46 Pa, followed by a decrease to a plateau associated with dynamic yield stress in the presence of imposed rotation. For a layer height (h) = 20 mm, the mathematical equation presented by Wangler et. al. [95] to assess the stability of the layer based on yield stress gives a minimum value of around 230 Pa, which is easily achieved by the MSWI-1 mixture in this work (Figure 9 (b)). The decreasing curve obtained in the hysteresis test was plot and the test curve data was linearly fitted in the range of 10 rpm to 35 rpm, which showed good relative stability, as shown in Figure 9 (b). From the Reiner-Riwlin equation [56, 96], the plastic viscosity and dynamic yield stress were found: 7.56 Pa · s and 265.44 Pa, respectively. It is important to note that the high static yield stress indicates strong resistance to flow at rest, which is essential for preserving the printed structure's shape between print intervals, while the dynamic yield stress governs pumpability and flow consistency during extrusion. The area enclosed between the up-and-down paths represents the energy dissipated due to internal structural changes during the shear cycle. This area quantifies the material's resistance to structural breakdown and its subsequent recovery ability under dynamic loading.

A prominent peak in shear stress at the beginning of the ramp-up phase, corresponding to the static yield stress, indicates strong inter-particle cohesion and a well-structured internal network at rest [97]. Following the peak, the shear stress declines and stabilizes during the high-speed steady state, representing the dynamic yield stress. The curve during the ramp-down phase shows partial structural rebuilding. The recovery is not complete at the end of the test time, and this is the typical property of a thixotropic material, where the process of flocculation takes longer than the process of breakdown. There is considerable thixotropy, indicating that the material has a significant degree of internal restructuring when subjected to shear. This rheological profile is beneficial for 3D printing. The recovery shown in the downward curve is partial, suggesting time-dependent thixotropy of which long rest times between layer depositions are not necessary for buildability.

The yield stress measurements are correlated with the particle flocculation, the slurry's free water content, and the mechanism of reaction [98]. Despite the fact that the rate of reaction of geopolymer mixes slows with a rise in MSWIBA, the presence of MSWIBA absorbs free water, which is present in the mixture, due to its irregular shape [47], corresponding to the rise in setting time with MSWIBA. The free water in the mixture is reduced, increasing its viscosity and shear stress and increasing the particle friction within the mixture.

Therefore, the choice of MSWI-1 as a 3D printing material suited to extrusion-based 3D printing is validated by the results of the hysteresis test as the material possesses good transition between static state and dynamic state and can recover its structure enough after terminating the shear process. The rheological behavior supports uninterrupted printing and good interlayer adhesion with minimal deformation, critical for additive manufacturing processes.

To quantify the viscosity recovery behavior after shear, the authors introduced the Viscosity Recovery Index (VRI), defined as the ratio (expressed in percentage) between the initial (pre-shear) apparent viscosity (step 1) and the post-shear (recovered) apparent viscosity (step 3). This index provides a percentage-based measure of the mix's ability to recover its structure after shearing. The higher the VRI value, the better the recovery will be, and this directly aligns with improved shape retention and buildability in the 3D printing process. Figure 9 (c) shows the frequency of occurrence of the normalized viscosity recovery (%).

Figure 9 (a) and (c) indicate that the VRI value is 86.85% for the MSWI-1 mix. A higher VRI indicates that the structure has been rebuilt more since the cessation of shear, necessary to maintain the form of the filaments. The higher the VRI, the quicker the viscosity returns to its original level after extrusion, which corresponds to better buildability and geometric stability. It minimizes the need for external supports or extended resting times between layers, thus enhancing printing speed and efficiency. The balance between static yield stress and VRI ensures that the mix retains its shape under its own weight while remaining extrudable through the nozzle without clogging.

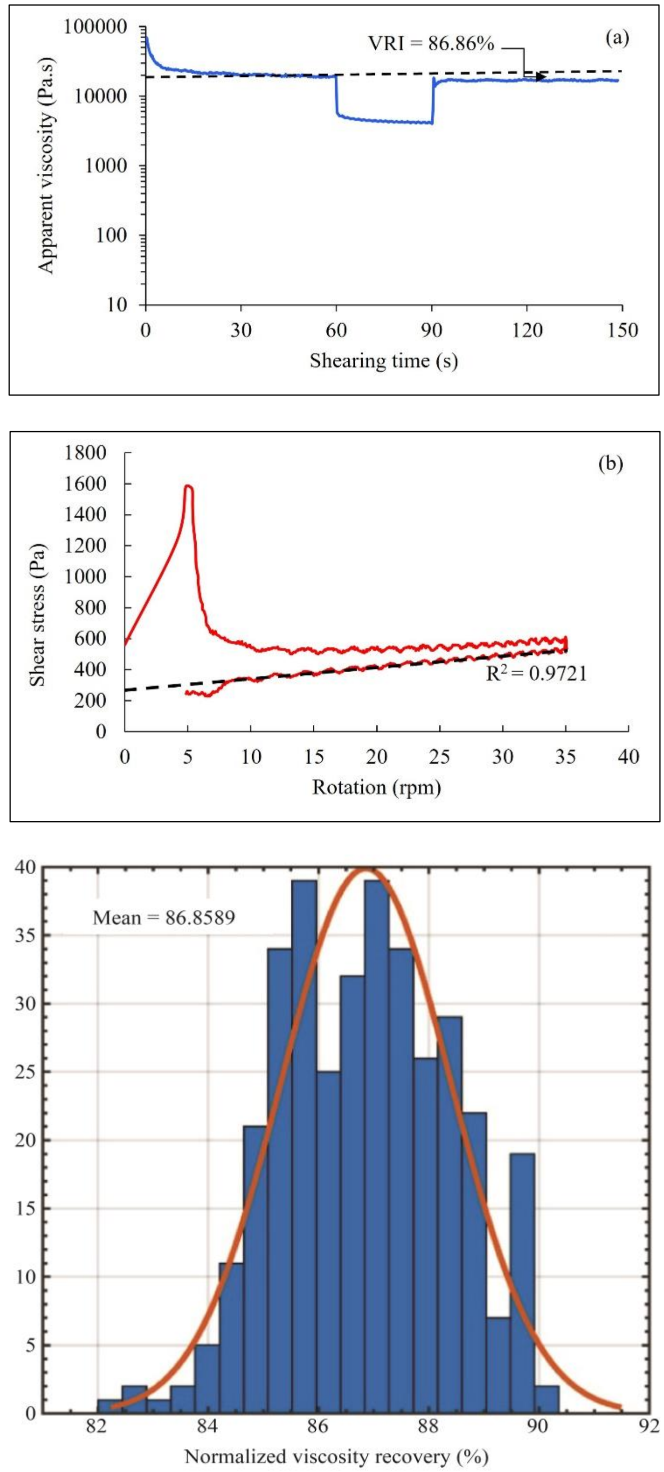

(c)

Fig. 9 (a) Viscosity recovery and (b) Rheological behavior of MSWI-1 mix, and (c) Normalized viscosity recovery (%) of MSWI-1 mix.

4.2. Hardened Properties

4.2.1. Compressive Strength

The findings of the compressive strength test carried on 3D printed geopolymer samples following a 28-day curing are presented in Figure 10. The strength measurements of 3D print specimens have been assessed in 3 orientations: perpendicular, lateral, and longitudinal, as observed in Figure 10 (a). Furthermore, the mold cast samples' compressive strength after curing for 28 days is presented in Figure 10 (b) to analyze the change in strength resulting from the printing method. The test results show that the MSWI-1 mixture containing 10% MSWIBA exhibited the greatest compressive strength, irrespective of the mold casting or printing directions. In contrast to the MSWI-0 mix, the 28-day strength of the MSWI-1 printed specimens exhibited increases of 5.96%, 2.47% and 1.3% in the longitudinal, perpendicular, and lateral orientations, respectively. In a comparable manner, the strength of mold cast samples exhibited an increase of 7.52% following a 28-day period. The rise in MSWIBA content exceeding 10% of the binder has caused a drop in the compressive strength of mold-cast samples. The MSWI-3 casted samples showed a decrease of about 20.4% in compressive strength after 28 days, in comparison to the MSWI-0 mixture. The decline in strength is because of the low amorphous content in MSWIBA, which leads to a reduced reaction rate of the MSWIBA precursor [48, 99, 100]. The slowly but steadily forming gel caused by the geopolymerization of fly ash and MSWIBA, which filled in some of the gaps and weak interlayers, may have lessened the noticeable anisotropy in the 3D-printed samples. Similar findings were reported in a recent study [101]. The strength properties diminish as the proportion of MSWIBA in the mixture rises. At 28 days, the assessed compressive strength characteristics for every mix surpass 25 MPa, suggesting that they are suitable for use in structural concrete applications.

Further, the strength in compression of the print samples in every tested direction is found to be lesser than corresponding mold cast samples. This may be a result of intrinsic voids that may occur during the printing technique with the use of a circular nozzle [82]. Therefore, compared to mold cast samples, the 3D print samples have a lesser strength in compression. Additionally, printed specimens are noticed to present anisotropic strength characteristics, with the strength values varying according to the testing directions, as reported in previous studies [102-104]. In all mixtures, the compressive strength was least in the lateral orientation, whereas the greatest in the longitudinal (printing) direction, as shown in Fig. 10 (a). Other researchers also reported similar patterns of compressive strength [56, 105]. The strong compaction in the direction of print brought on from the exerted pressure by the extrusion method is responsible to provide the printing direction its high strength attributes. On the other hand, a weakened intermediate layer with more voids or porosity within the subsequent layers printed may be linked to the lateral direction's least strength in compression [106, 107].

For statistical analysis of the compressive strength results to determine if the differences between mixtures are statistically significant, the Friedman's rank sum test is used to check the significant difference between the selected MSWIBA mixes. The non-parametric testing results are shown in Table 4. The null-hypothesis of Friedman's test shows the equivalency of all MSWIBA mixes. Table 4 (a) shows the mean rank of MSWIBA mixes, and it is also reflected in Figure 11. Figure 11 shows the individual MSWIBA mixes' statistical information graphically. The p-value indicates a performance difference between all selected MSWIBA mixes, as it comes out to be less than 0.05, as shown in Table 4 (b). Hence, the selected MSWIBA mixes are substantially different in their performances. The decisive observations obtained from experimental studies of these MSWIBA mixes are therefore uniquely significant.

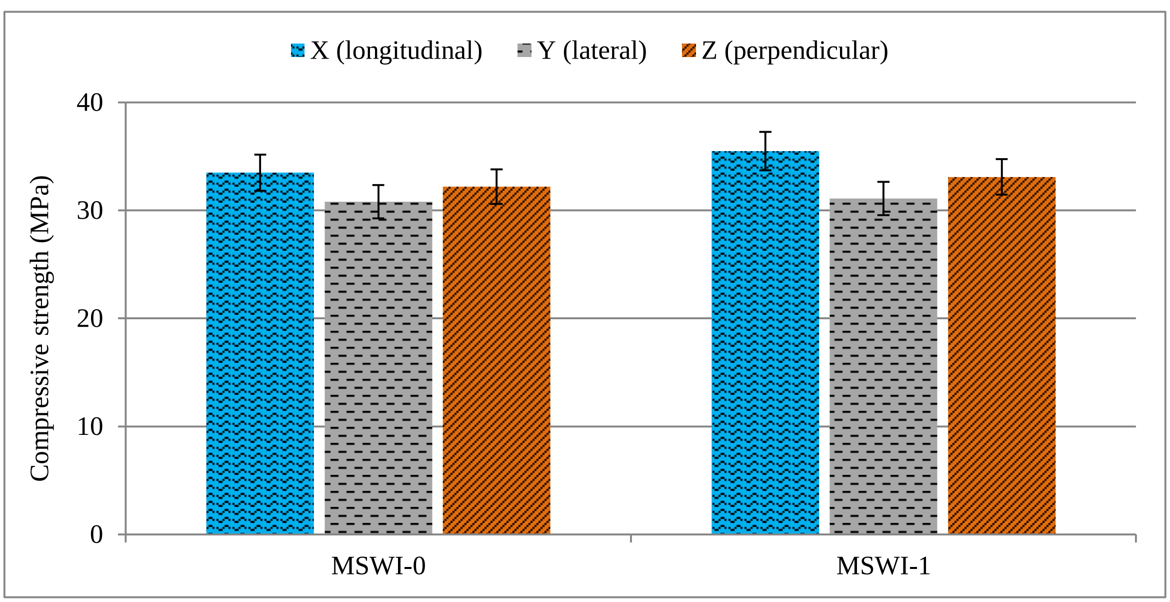

(a)

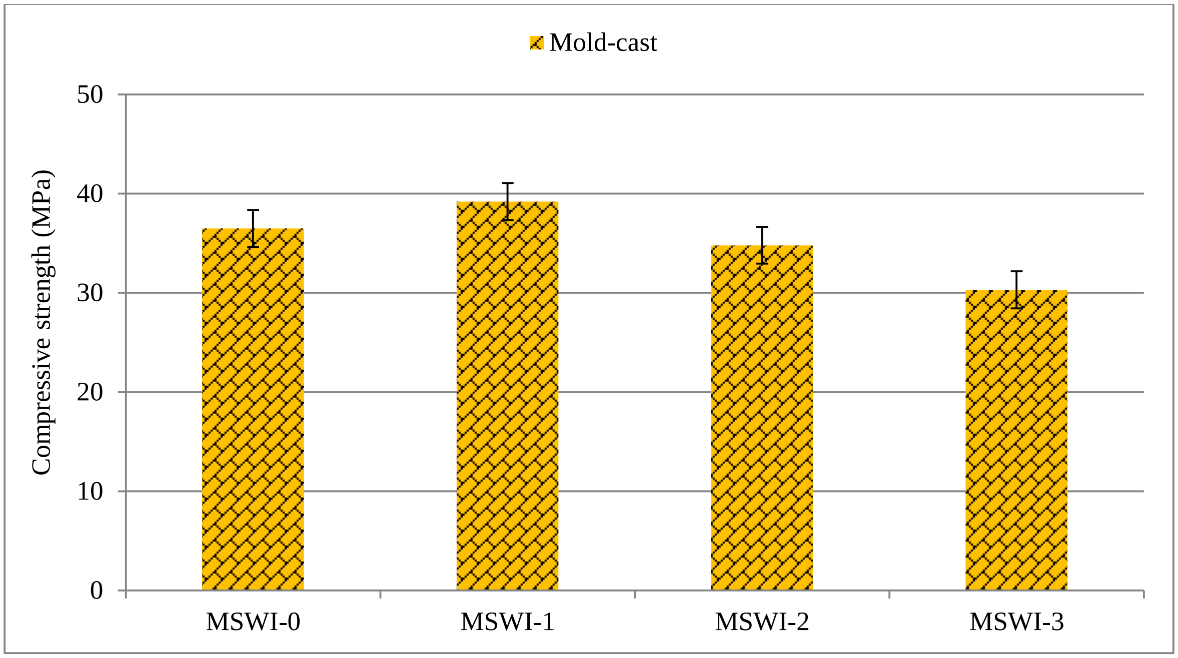

Fig. 10 Compressive strength of (a) Print samples (in different orientations) and (b) Mold cast samples for the formulated mixtures.

Table 4. Friedman's test results

(a) Ranks		**(b) Test statistics**	
	Mean rank	N	6
Mold-cast	3.83	Chi-Square	12
X (longitudinal)	2.83	Degree of freedom	3
Y (lateral)	1.5	Asymptotic Significance (p)	0.007
Z (perpendicular)	1.83		

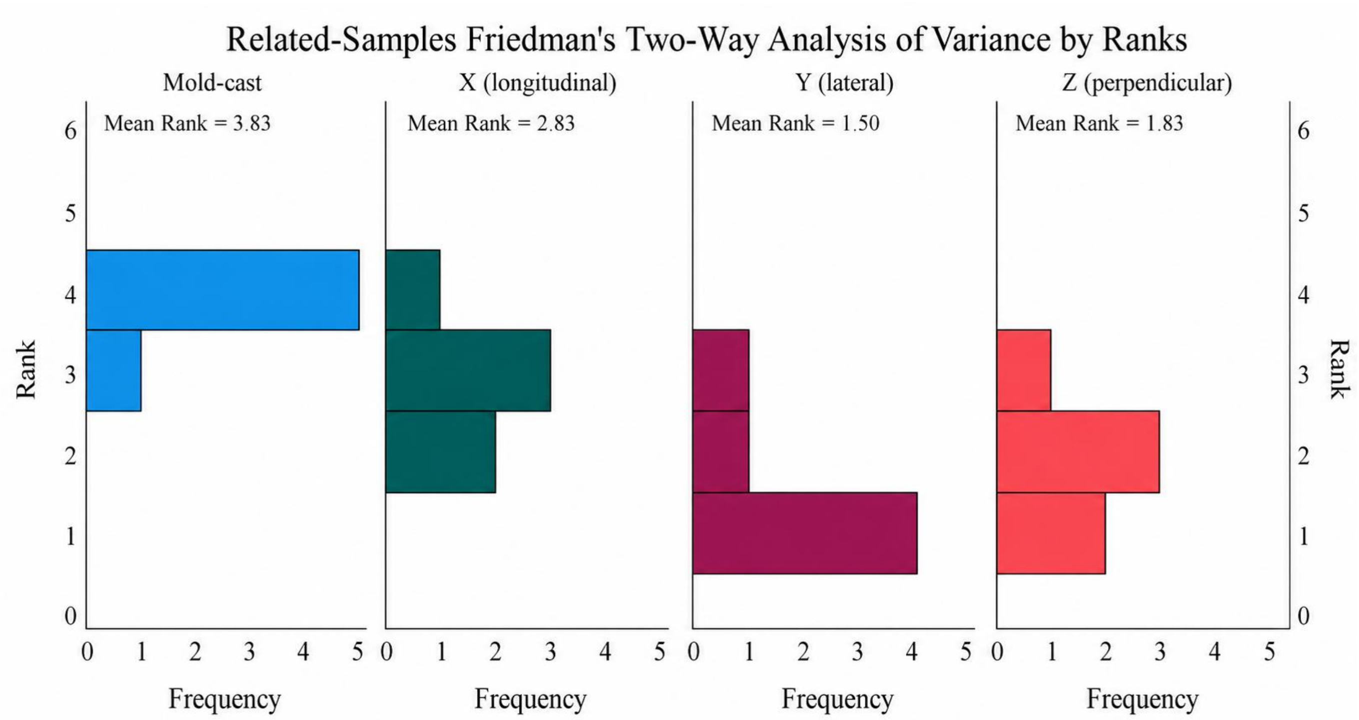

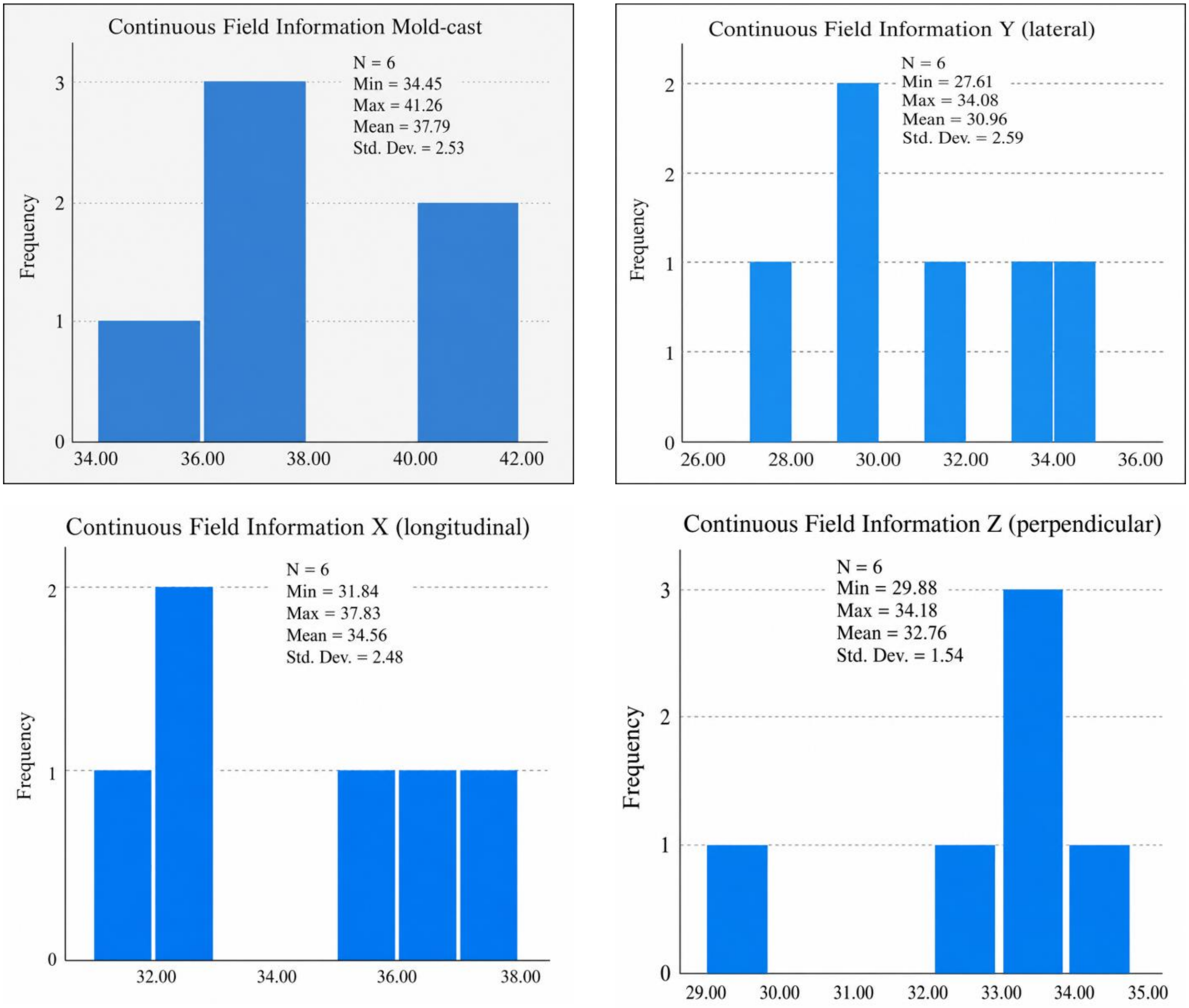

Fig. 11 Graphical representation of statistical information for the compressive strength of the formulated mixtures

4.2.2. Physical Properties

The average density of mold-cast and printed specimens for the formulated mixtures is compared in Figure 12. Since the MSWIBA ashes possess lower specific gravity and porous nature, there may have been a modest decrease in density as a result of their inclusion [108].

The MSWI-1 mixture printed specimen had a little lower average density (2025 kg/m^3) in comparison to the mold-cast counterpart, which had an average density of 2155 kg/m^3.

This is probably because the layer-on-layer extrusion technique inevitably creates voids in-between printed layers [109]. However, this observation was in contrast to that reported in a study [110].

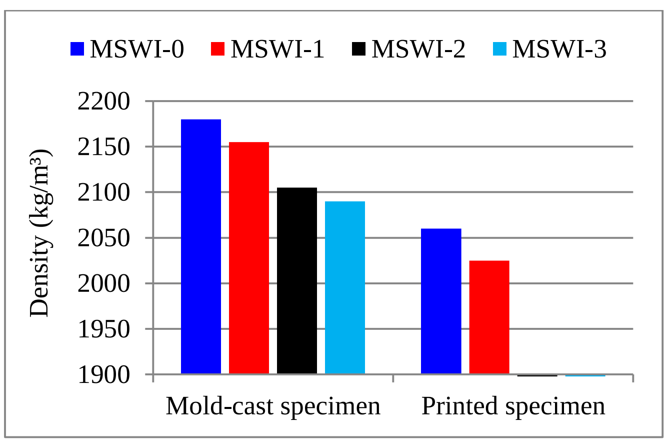

Fig. 12 Average density of mold-cast and print samples for the formulated mixtures

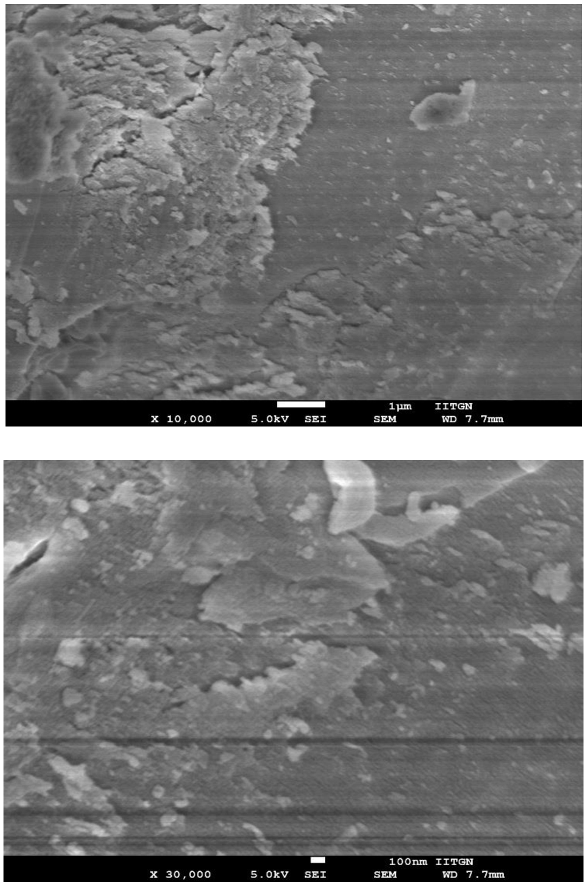

Fig. 13 SEM images of MSWI-1 mixture

4.3. Microstructure Characterization

After 28 days of curing, the printed mix MSWI-1's microstructural examination showed the existence of aluminosilicate gel, as seen in Figure 13. The FESEM images show two distinguished zones: the dense and compact gel appearing in a smooth, darker grey shade, while the rough, lighter grey shade represents the particles of unreacted MSWIBA. Although a small amount of unreacted MSWIBA particles is visible in the FESEM images due to its low reactivity [111, 112] whereas its irregularly shaped particles, having a porous nature, could have led to inadequate bonding, causing microcracks [113, 114] as seen in the FESEM images. An overall uniform and dense hardened microstructure is observed for the MSWI-1 mix.

4.4 Environmental Assessment

4.4.1. Environmental impact

Calculations were performed to examine the comparison between a printable composition containing cement and this work's optimal MSWI-1 composition in terms of the energy consumed and CO_2 released. The mixing combinations of printed concrete composition and constituents' life span assessment values gleaned from pertinent publications are presented in Table 4.

The consumed energy and CO_2 discharged related to the manufacturing of 1m^3 of printable composition containing cement and optimal printable MSWI-1 composition are shown in Figures 14 and 15. To synthesize the 3D printing geopolymer mix, the powder activator was the primary participant, accounting for approximately 34.37% of the CO_2 emissions and 72.38% of the total embodied energy, when taking into account the distinct roles that various components play in creating an impact on the environmental. About 40.65% of the CO_2 emissions and 8.73% of the total embodied energy linked to the formulation of the 3D printed geopolymer came from the MSWIBA. Nevertheless, for the OPC printable mixture, the OPC was the primary cause of 83.33% of the CO_2 released and 73.66% of the total energy embodied related to the synthesis of the 3D printing OPC mix.

Table 5. Mixing combinations of printable compositions containing cement and optimal MSWI-1 composition, and embodied energy and CO_2 emission details of constituents

Constituents	3D printable OPC mixture [82] (kg/m^3) (Mix-2)	3D printable geopolymer concrete mixture (kg/ m^3) (mix MSWI-1)	CO_2 emissions (kg/kg)	Embodied energy (MJ/ kg)
Cement	290.0	-	0.85 [115]	4.80 [115]
Fly ash	278.0	272.27	0.0196 [116]	0.05 [117]
GGBS	-	340.51	0.0265 [116]	0.33 [118]
MSWIBA	-	68.10	1.1 [119]	2.16 [119]
Silica fume	145.0	-	0.014 [120]	0.10 [120]
Solid activator	-	68.10	0.93 [121]	17.90 [121]
Silica sand	1211.0	1017.35	0.026 [122, 123]	0.175 [122, 123]
Retarder	-	6.8	0.307 [124]	0.822 [124]
Superplasticizer	7.0	-	1.48 [122, 123]	36.76 [122, 123]

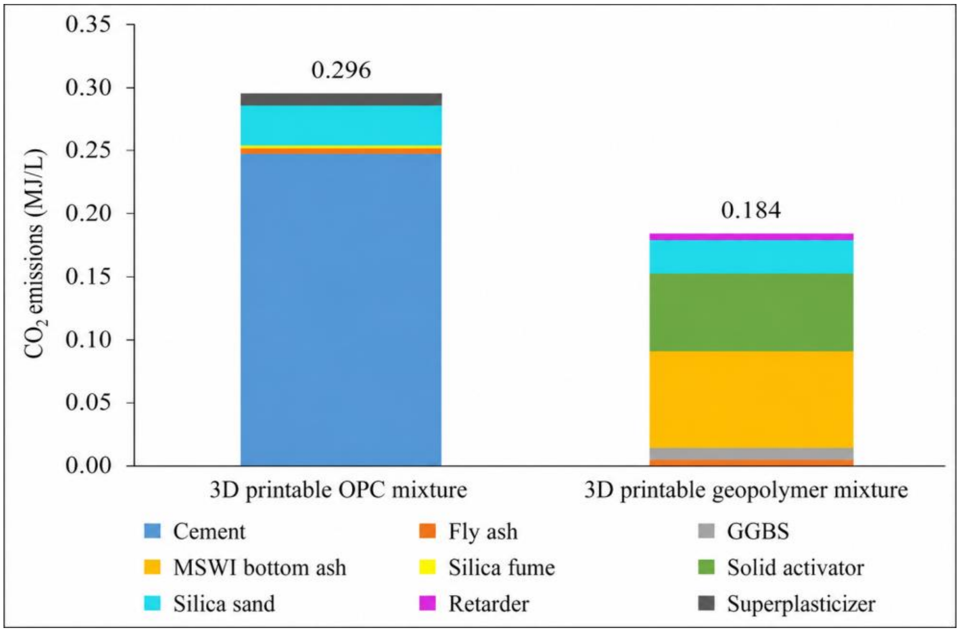

Fig. 14 CO_2 emissions calculated for printable composition containing cement and optimal MSWI-1 composition

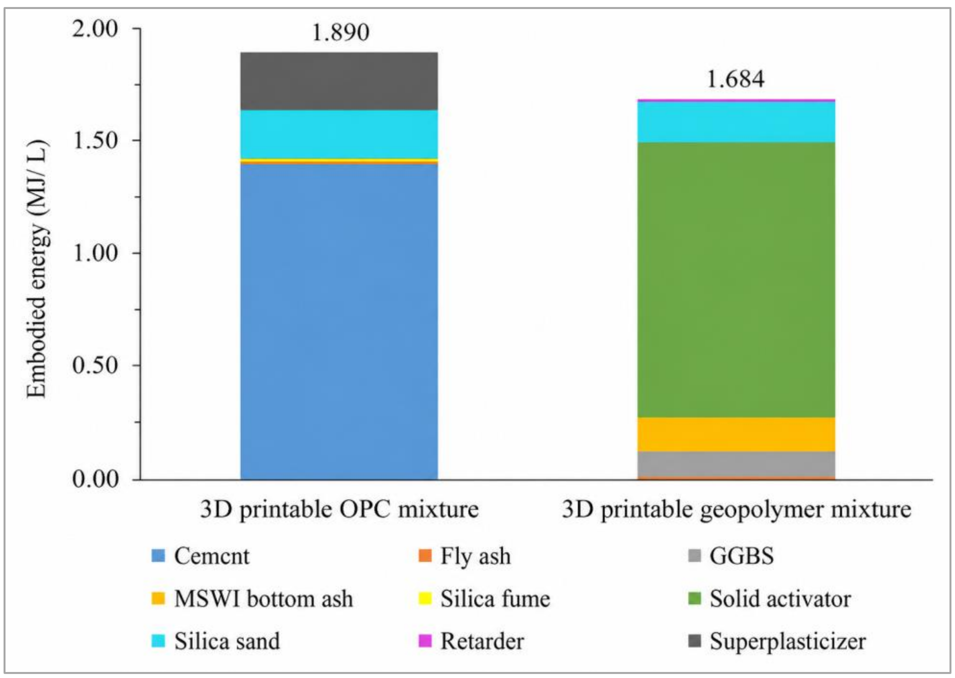

Fig. 15 Embodied energy calculated for printable composition containing cement and optimal MSWI-1 composition

The manufacturing of $1m^3$ of the optimal 3D printed MSWI-1 formulation prepared during the current work resulted in CO_2 emissions and embodied energy that were 38% and 11% lower, respectively, than those of the 3D print OPC composition, as shown in Figures 14 and 15. This is because the 3D printed MSWI-1 mixture's raw constituents, synthesized at room temperature, fully replaced the elevated CO_2 and energy-consumptive printable composition containing cement. Thus, the developed 3D printed one-part geopolymer can be deemed a sustainable substitute for the 3D printed OPC mix, offering similar mechanical qualities but 11% lower consumption of energy and 38% lower CO_2 emissions.

4.4.2. Life Cycle Assessment

Life Cycle Assessment (LCA) was conducted to quantify the environmental performance of the formulated 3D-printed one-part geopolymer concrete incorporating fly ash, GGBS, and MSWIBA. An evaluation based on the cradle-to-gate system boundaries was used [125], considering raw material acquisition, transporting, processing of industrial by-products, production of dry alkaline activators, and manufacturing of 1 m^3 of printable concrete. The functional unit selected for the analysis was 1 m^3 of printable concrete, enabling a direct comparison with the conventional 3D printed OPC mixture.

The developed one-part geopolymer system completely eliminates Portland cement by utilizing FA, GGBS, and MSWI-BA as aluminosilicate precursors. These industrial and municipal by-products require substantially lower processing energy than clinker production, thereby significantly reducing the embodied carbon associated with binder production. Besides, for one part, geopolymer uses a solid activator, which does not need to use dangerous liquid alkaline solution and does not need to be transported on site and stored. Sucrose powder is used as a retarder that further improves the printability of the ink without causing substantial environmental problems in view of the low quantity of the retarder.

According to life cycle assessment findings, the alkaline activator has the most significant influence on the environmental consequences of the geopolymer combination. According to the life cycle assessment results, the primary source of the geopolymer mixture's negative effects on the environment is its manufacture as a dry alkaline activator [126]. Anhydrous sodium metasilicate is a major contributor to the total CO_2 emissions, with around 34.37%, and the embodied energy contributor for 1 m^3 of printable geopolymer mixture is around 72.38%. While only a small proportion of the total mass, the high energy demands to produce the activator can make a big difference to the overall environmental footprint of one-part geopolymer systems. MSWIBA also made an important part in the effect on the environment due to the energy used in collecting, drying, grinding, sieving and processing. The contribution of CO_2 emissions due to the production and use of MSWIBA was around 40.65% and 8.73% of total embodied energy of the geopolymer mixture, respectively. However, it can result in an enormous decrease in municipal solid waste landfilling [66], and the material is a valuable building block, which helps in relation to the tenets of the circular economy and decreases the need for virgin materials.

MSWIBA, being part of WtE process, does not resemble any other cement or manufactured material like GGBS. Because of the inherent heterogeneity of MSWIBA, in particular, from WtE plants, the initial condition of the waste can differ significantly between locations and times. Therefore, the process of pre-processing (e.g., drying, grinding and sieving) is highly case dependent and cannot be applied to all cases. Adding processing-related emissions and energy demand for MSWIBA to Table 4 of the revised version would suggest a fixed and repeatable process, thus potentially misrepresenting variability in the real world. Furthermore, as WtE plant technologies improve, the quality of MSWIBA is continuously rising, and some plants may even be able to supply pre-processed, ready-to-use MSWIBA in the near future. The trend coincides with the circular economy objectives in the world, and it is expected that the need for further processing will be minimized or even eliminated, which will result in nearly negligible emissions associated with the processing. Moreover, in large-scale applications, the energy requirement per unit MSWIBA is drastically reduced because of scale economies. The efficient use of this, combined with the valorisation of the waste product, which would otherwise be dumped in landfills, highlights the low net environmental impact of MSWIBA. For this reason, localized and potentially non-essential MSWIBA processing stages were intentionally omitted from Table 4 so as to keep the current study structurally consistent and comparable with other studies, as well as generalizable to the broader MSWIBA processing. This is consistent with best practice in LCA for secondary and waste-derived materials, where the environmental burdens typically are attributed to the main product (in this case, energy generation) while the secondary by-product (MSWIBA) is assumed burden-free or burdened to a minimum. Nevertheless, the generalized values for processing MSWIBA are not included in Table 4, as this would create the impression of quantification if using a highly variable scenario.

The traditional printable OPC mixture, on the other hand, had an overwhelming dominance of the manufacture of OPC. Around 83.33% of the total CO_2 discharged and 73.66% of the total embodied energy of 1m^3 of printable concrete was provided by OPC. These values are mostly due to the limestone calcination and the elevated temperature process of clinker production, which are known to be the other significant sources of GHG emissions and fossil fuel consumption in the world.

The results of the direct comparison between the optimized printable geopolymer formulation (MSWI-1) and the printable OPC mixture show good evidence of the environmental benefits of the proposed formulation. The optimized 3D-printed one-part geopolymer was approximately 38% less CO_2-intensive and 11% less embodied energy compared to the 3D-printable OPC. The significant amount of GHG reduction demonstrates that industrial and municipal solid waste-derived precursors are an effective approach to reduce GHG emissions of additively manufactured cementitious materials when contrasted to OPC.

The embodied energy is found to be still considerable, even though it is not as large as the reduction in carbon emissions; it shows that the energy demand of the manufacturing of the alkaline activator has not been reduced sufficiently. Thus, additional research is needed for the development of lower-energy solid activators and other activation methods for further enhancing the environmental performance of one-part geopolymer systems.

In addition to carbon emission and energy savings, the developed geopolymer also has tremendous resource conservation benefits. By using the complete replacement of Portland cement, the amount of limestone extracted and the production of clinker are reduced, and by using FA, GGBS and MSWI-BA, large-scale recycling of industrial and municipal solid wastes becomes promoted. This circular waste valorisation strategy minimizes the landfill demand, saves natural resources and also decreases waste disposal pollution. Moreover, the developed one-part geopolymer does not require any extra energy for thermal curing, which is customary for conventional geopolymer materials since the material is ambient-cured. The use of dry activators also improves occupational safety by avoiding highly alkaline liquid solutions during material preparation and printing operations.

In comparison to traditional printable OPC concrete, the suggested 3D-printed one-part geopolymer concrete is more practical and beneficial to the environment, according to the life cycle assessment. An efficient use of industrial and municipal solid wastes, along with a decrease in greenhouse gas emissions, embodied energy, cement use, and landfill disposal, provides credence to the idea that this material could be used for sustainable additive manufacturing in the building industry. These results contribute directly to the accomplishment of Sustainable Development Goal 9, 11, 12, and 13, and are in line with green chemistry, resource efficiency, and the circular economy principles.

4.5. Discussion

The performance of the synthesized one-part MSWIBA geopolymer is comparable to recent state-of-the-art research on waste-derived printed geopolymers. Prior research has primarily been on cast MSWIBA-based geopolymers or two-part alkali-activated systems, with a principal focus on compressive strength and microstructural analysis. This work systematically combines rheological characterization, printability assessment, anisotropic mechanical behavior and environmental evaluation into a single framework. The optimum MSWI-1 mix has enhanced printability because of the balanced interaction of fly ash, GGBS and 10% MSWIBA. Fly ash improves flowability due to its spherical particle shape, whereas GGBS enhances geopolymerization and early structural development by promoting C–A-S-H gel formation. The substitution of 10% MSWIBA for fly ash improves particle interlocking and structural reconstruction after extrusion, which results in enhanced thixotropy and viscosity recovery, both of which are crucial to layer stability during printing. Any increase of the MSWIBA concentration more than the optimum amount produces an excess of irregular and porous particles, which demand more water, thus reducing the workability and limiting the formation of the geopolymer gel, eventually reducing the compressive strength. The successful printing of a structure of 600 mm height without failure proves the immediate effect of the improved rheological properties on the buildability. Moreover, the decrease in embodied energy and carbon emissions indicates that these performance improvements are achieved while improving the environmental sustainability of the material simultaneously, thus providing a promising route for the utilization of MSWIBA in extrusion-based digital construction.

4.5.1. Regulatory Frameworks, Standard Codes, and Practical Implementation Pathways

For any innovative 3D printable composite to transition from a laboratory environment to field-scale structural applications, it must navigate a complex matrix of environmental regulations, material codes, and practical engineering constraints. The deployment of the one-part MSWIBA geopolymer developed in this study carries significant implications across these three domains.

Environmental Regulatory Compliance and Waste Diversion

Regarding waste management policy, the study is in agreement with the statutory requirements of SWMR, 2026, enacted by MoEFCC. These revisions impose stringent legal restrictions on landfilling and mandate the integration of municipal waste streams into industrial co-processing and circular economy infrastructure. The ink design offers a high volume diversion mechanism for municipal byproducts through use of MSWIBA as a partial precursor.

Standardization Obstacles and Performance-based Testing Codes

The key technical obstacle [127] to the widespread commercial use of 3D printable geopolymers is the prescriptive nature of legacy building codes. Current structural concrete standards (e.g. IS 456 in India, ACI 318 in the US, Eurocode 2) are basically based on Ordinary Portland Cement (OPC) binders and conventional formwork deposition. They do not permit the anisotropic mechanical properties typical of layered additive manufacturing. To overcome these limitations and to move towards standardization, a performance-based testing approach should be used. The material developed in this work is in agreement with the emerging alternative framework:

- *Precursor characterization:* Standard fly ash and GGBS are governed by IS 3812 and IS 12089, respectively. Inclusion of processed MSWIBA warrants comparison with broader specifications like ASTM C1866 that address non-traditional aluminosilicate inputs.
- *Fresh-state printing metrics:* Traditional workability tests do not include dynamic behaviors needed for automated extrusion. This work is based on the basic rheological parameters, i.e. static yield stress variation, apparent viscosity and thixotropic recovery, following the testing recommendations in the available literature [79, 95, 128, 129]. This set of performance indicators provides code-drafting bodies with quantifiable measures to evaluate structural buildability.

Field implementation and Digital Construction Scalability

From a practical point of view, the transition from a “two-part” geopolymer system (which requires liquid chemical activators) to the “one-part” dry-mix formulation developed here is a huge step forward for the on-site implementation. In the case of two-part geopolymers, highly corrosive chemical solutions which are viscous have to be handled, transported and dosed precisely on the construction site. This creates severe occupational safety hazards and systemic errors in automated mixing pumps.

The formulation lends itself to a simple “just-add-water” protocol by including anhydrous sodium metasilicate powder directly in the dry precursor blend (fly ash, GGBS, MSWIBA and sucrose retarder). This enables the mix to be processed through conventional batch plants and the continuous 3D concrete printing delivery systems currently in use by the construction industry. The success of extrusion of the 600-mm high continuous structure shows that the structural open-time, layer-to-layer bond, and early-age strength of this configuration are fully compatible with existing gantry and robotic-arm extrusion systems. This compatibility confirms the feasibility of using this eco-efficient material for large-scale, automated infrastructure elements.

5. Conclusion and Future Research Directions

For digital construction applications, the present research focuses on the viability of using MSWIBA as a precursor for 3D printing of geopolymer concrete. It was evaluated how the MSWIBA content affected the geopolymer’s fresh and hardened features suitable for concrete 3D printing. The key takeaways from this research are as follows:

- The flowability of the mixes declined as the MSWIBA concentration grew, while the rise in MSWIBA content prolonged the setting time of the mixes.
- Good thixotropy and viscosity recovery characteristics, which are necessary for the intended printability, were displayed by the optimum mixture MSWI-1. The 600 mm tall cylindrical structure was successfully printed, demonstrating the optimal mixture's substantially enhanced buildability.
- The 3D printed specimens’ compressive strength showed anisotropic behavior; the recorded strength was least in the lateral direction, whereas it was maximum in the longitudinal (printing) direction.
- When the MSWIBA proportion is raised by up to 10%, the compressive strength of 3D printable concrete increases, while reduced compressive strength properties result from a further rise in the MSWIBA content.
- In comparison to traditional Portland cement concrete, the embodied energy and carbon footprint of 3D printable geopolymer concrete is reduced by 11–38%.

The study revealed the excellent potential of MSWIBA as a sustainable precursor for the production of one-part 3D printable geopolymer concrete. The determined fresh and hardened properties, and the proved environmental benefits, confirm the feasibility of this method for digital construction. But some limitations are mentioned, and the future research directions are suggested to provide broader practical implementation and extend the present findings as follows:

- *Material variability and reactivity:* The MSWIBA used in this study was only mechanically processed without any chemical pre-treatment. MSWIBA is a highly variable and heterogeneous material with variable reactivity, so future studies are needed to assess the effect of the source variability and whether it can be enhanced through pre-treatment (thermal activation or chemical stabilization).
- *Regulatory compliance and environmental safety:* Even though the mechanical and rheological performances were studied in this work, the long-term environmental behavior of 3D printed one-part geopolymer concrete incorporating MSWIBA should be carefully investigated, such as the potential to leach out heavy metals and soluble salts.
- *Durability performance:* Early-age and 28-day mechanical properties of the material were evaluated. Future research should focus on studying the durability properties of 3D printed MSWIBA-based geopolymer concrete under various environmental conditions, such as resistance to freeze-thaw, acid and sulphate attack, carbonation, chloride penetration, heavy metal leaching, and drying-wetting cycles, to evaluate the long-term performance potential of MSWIBA-based geopolymer concrete.
- *Structural and geometric complexity:* The 3D printing trials were carried out on a lab-scale cylindrical geometry. The printability and the structural performance of more complex geometries and larger-scale elements need to be explored in future work to evaluate print integrity, dimensional accuracy and interlayer bonding in practice.
- *Reinforcement integration:* The present study doesn't involve reinforcement, which is significant for load-bearing and flexural performance in structural applications. Additional studies should focus on reinforcement methods that are compatible with 3D printing, such as fiber addition or hybrid reinforcement systems.

To conclude, although the present study confirms the viability of the utilization of MSWIBA as a 3D printable one-part geopolymer concrete, future studies should focus on further improving the robustness, applicability and industrial scalability of this sustainable construction method.

Conflicts of Interest

The authors declare that there is no conflict of interest regarding the publication of this paper.

Funding Statement

This research did not receive any specific grant from funding agencies in the public, commercial, or not-for-profit sectors.

Acknowledgments

Authors acknowledge the support from the Cretebots Digital Constructions Private Limited, Pune, Maharashtra, India, for 3D printing facility.

CRediT Authorship Contribution Statement

Prasad Barve: Writing – original draft, Visualization, Validation, Methodology, Resources, Investigation, Formal analysis, Data curation, Conceptualization. Santosh Shah: Writing – review & editing, Visualization, Validation, Supervision, Conceptualization. Deep Upadhyaya: Writing – review & editing, Visualization, Validation, Supervision, Project administration.

References

[1] Tuan D. Ngo et al., "Additive Manufacturing (3D Printing): A Review of Materials, Methods, Applications and Challenges," *Composites Part B: Engineering*, vol. 143, pp. 172-196, 2018. [CrossRef] [Google Scholar] [Publisher Link]

[2] Nhi Tran et al., "Eco-Friendly 3D-Printed Concrete Using Steel Slag Aggregate: Buildability, Printability and Mechanical Properties," *International Journal of Concrete Structures and Materials*, vol. 18, no. 1, pp. 1-18, 2024. [CrossRef] [Google Scholar] [Publisher Link]

[3] Jianyu Shen et al., "Mechanical and Thermal Properties of 3D Printed Earth Concrete Solidified by Geopolymers: A Study of Utilizing Excavated Clay," *Journal of Building Engineering*, vol. 107, 2025. [CrossRef] [Google Scholar] [Publisher Link]

[4] Jian-nan Li et al., "Enhancing Thermo-Mechanical and Moisture Properties of 3D-Printed Concrete through Recycled Ultra-Fine Waste Glass Powder," *Journal of Cleaner Production*, vol. 480, 2024. [CrossRef] [Google Scholar] [Publisher Link]

[5] Hao Lucen et al., "Development of CO2-Activated Interface Enhancer to Improve the Interlayer Properties of 3D-Printed Concrete," *Cement and Concrete Composites*, vol. 162, 2025. [CrossRef] [Google Scholar] [Publisher Link]

[6] Meiyan Bai et al., "Interfacial Bond Properties between 3D Printed Engineered Cementitious Composite (ECC) and Post-Cast Concrete," *Cement and Concrete Composites*, vol. 157, 2025. [CrossRef] [Google Scholar] [Publisher Link]

[7] Mohammad Rasul GivKashi et al., "Effect of Pumping Process on the Properties of 3D Printed Concrete Containing Air-Entraining Agent," *Journal of Sustainable Cement-Based Materials*, vol. 14, no. 3, pp. 466-476, 2025. [CrossRef] [Google Scholar] [Publisher Link]

[8] L. Hass, F.P. Bos, and T.A.M. Salet, "Bond Governed Interactions between Helical Reinforcement and 3D Printed Concrete," *Journal of Building Engineering*, vol. 99, pp. 1-28, 2025. [CrossRef] [Google Scholar] [Publisher Link]

[9] Xiangpeng Cao, Shuoli Wu, and Hongzhi Cui, "Experimental Study on In-situ Mesh Fabrication for Reinforcing 3D-Printed Concrete," *Automation in Construction*, vol. 170, 2025. [CrossRef] [Google Scholar] [Publisher Link]

[10] Alise Sapata et al., "Establishing Benchmark Properties for 3D-Printed Concrete: A Study of Printability, Strength, and Durability," *Journal of Composites Science*, vol. 9, no. 2, pp. 1-23, 2025. [CrossRef] [Google Scholar] [Publisher Link]

[11] Mary Meisenzahl, This Building in Dubai is the Largest 3D-printed Structure in the world — And it Took Just 3 Workers and a Printer to Build it, Business Insider, 2019. [Online]. Available: https://www.businessinsider.com/dubai-largest-3d-printed-building-apis-cor-photos-2019-12/

[12] Monique Randolph, Bringing Innovation to Fruition: Marines 3D Print 1st Reinforced Concrete Bridge in Western Hemisphere, Office of Public Affairs and Communication, Marine Corps Systems Command, 2019. [Online]. Available: https://www.marcorsyscom.marines.mil/News/News-Article-Display/Article/1742621/bringing-innovation-to-fruition-marines-3d-print-1st-reinforced-concrete-bridge/#:~:text=%E2%80%9CMaking%20homes%20that%20don't,the%20beginning%20of%20our%20progress.%E2%80%9D

[13] World's First 3D Printed Large Concrete Tanks Made with Materials Savings Of 25%, COBOD, 2024. [Online]. Available: https://cobod.com/worlds-first-3d-printed-large-concrete-tanks-made-with-materials-savings-of-25/

[14] The World's Largest Concrete 3D Printed Pedestrian Bridge, Tsinghua University News, 2019. [Online]. Available: https://www.tsinghua.edu.cn/en/info/1244/2966.htm

[15] India's and the World's First 3d Printed Post Office Made By Construction Giant L&T Construction Praised By Modi, India's Prime Minister, COBOD, 2023. [Online]. Available: https://cobod.com/indias-and-the-worlds-first-3d-printed-post-office-made-by-construction-giant-lt-construction-praised-by-modi-indias-prime-minister/

[16] Wahid Ferdous et al., "Recycling of Landfill Wastes (Tyres, Plastics and Glass) in Construction – A Review on Global Waste Generation, Performance, Application and Future Opportunities, Performance," *Resources, Conservation and Recycling*, vol. 173, 2021. [CrossRef] [Google Scholar] [Publisher Link]

[17] Kirubajiny Pasupathy, Sayanthan Ramakrishnan, and Jay Sanjayan, "3D Concrete Printing of Eco-Friendly Geopolymer Containing Brick Waste," *Cement and Concrete Composites*, vol. 138, pp. 1-11, 2023. [CrossRef] [Google Scholar] [Publisher Link]

[18] "*Annual Report 2022-23 on Implementation of Solid Waste Management Rules, 2016*," Central Pollution Control Board (CPCB), Delhi, India, 2023. [Publisher Link]

[19] Waste to Energy, Press Information Bureau Government of India Planning Commission, 2014. [Online]. Available: https://www.pib.gov.in/newsite/PrintRelease.aspx?relid=105057&reg=48&lang=2

[20] CIRCULAR ECONOMY in Municipal Solid and Liquid Waste, Ministry of Housing and Urban Affairs, Government of India, 2021. [Online]. Available: https://www.mohua.gov.in/static/uploads/2025/10/f090e493ba8d094ec2452d8d2cd0f2c3.pdf

[21] "*Annual Report 2020-21 on Implementation of Solid Waste Management Rules, 2016*," Central Pollution Control Board (CPCB), pp. 288-446, 2016. [Publisher Link]

[22] Ranjith Kharvel Annepu, "*Sustainable Solid Waste Management in India*," Master Thesis, Columbia University, pp. 1-189, 2012. [Google Scholar] [Publisher Link]

[23] Solid Waste Management Rules, 2026. [Online]. Available: https://cwas.org.in/resources/file_manager/Solid%20Waste%20Management%20Rules,%202026.pdf

[24] Hefa Cheng, and Yuanan Hu, "Municipal Solid Waste (MSW) as a Renewable Source of Energy: Current and Future Practices in China," *Bioresource Technology*, vol. 101, no. 11, pp. 3816-3824, 2010. [CrossRef] [Google Scholar] [Publisher Link]

[25] Paul H. Brunner, and Helmut Rechberger, "Waste to Energy–key Element for Sustainable Waste Management," *Waste Management*, vol. 37, pp. 3-12, 2015. [CrossRef] [Google Scholar] [Publisher Link]

[26] Nathan Curry, and Pragasen Pillay, "Biogas Prediction and Design of a Food Waste to Energy System for the Urban Environment," *Renewable Energy*, vol. 41, pp. 200-209, 2012. [CrossRef] [Google Scholar] [Publisher Link]

[27] Lidia Lombardi, Ennio Carnevale, and Andrea Corti, "Analysis of Energy Recovery Potential using Innovative Technologies of Waste Gasification," *Waste Management*, vol. 32, no. 4, pp. 640-652, 2012. [CrossRef] [Google Scholar] [Publisher Link]

[28] Wu-Jian Long et al., "Recycled use of Municipal Solid Waste Incinerator Fly Ash and Ferronickel Slag for Eco-Friendly Mortar through Geopolymer Technology," *Journal of Cleaner Production*, vol. 307, 2021. [CrossRef] [Google Scholar] [Publisher Link]

[29] Byeong-Hun Woo et al., "Utilization of Municipal Solid Waste Incineration Bottom Ash as Fine Aggregate of Cement Mortars," *Sustainability*, vol. 13, no. 16, pp. 1-12, 2021. [CrossRef] [Google Scholar] [Publisher Link]

[30] Arijeet Karmakar et al., "A Comprehensive Insight into Waste to Energy Conversion Strategies in India and its Associated Air Pollution Hazard," *Environmental Technology & Innovation*, vol. 29, pp. 1-20, 2023. [CrossRef] [Google Scholar] [Publisher Link]

[31] Zhenghui Phua et al., "Characteristics of Incineration Ash for Sustainable Treatment and Reutilization," *Environmental Science and Pollution Research*, vol. 26, pp. 16974-16997, 2019. [CrossRef] [Google Scholar] [Publisher Link]

[32] Hossam F. Hassan, "Recycling of Municipal Solid Waste Incinerator Ash in Hot-Mix Asphalt Concrete," *Construction and Building Materials*, vol. 19, no. 2, pp. 91-98, 2005. [CrossRef] [Google Scholar] [Publisher Link]

[33] Cristina Marieta, Ana Guerrero, and Iñigo Leon, "Municipal Solid Waste Incineration Fly Ash to Produce Eco-Friendly Binders for Sustainable Building Construction," *Waste Management*, vol. 120, pp. 114-124, 2021. [CrossRef] [Google Scholar] [Publisher Link]

[34] David Suescum-Morales et al., "Effect of Incorporating Municipal Solid Waste Incinerated Bottom Ash in Alkali-Activated Fly Ash Concrete Subjected to Accelerated CO2 Curing," *Journal of Cleaner Production*, vol. 370, pp. 1-17, 2022. [CrossRef] [Google Scholar] [Publisher Link]

[35] Yang Nan et al., "A Review of Research on the Valorization and Risk Management of Municipal Solid Waste Incineration Bottom Ash," *Materials*, vol. 19, no. 7, pp. 1-27, 2026. [CrossRef] [Google Scholar] [Publisher Link]

[36] Meixi Chen et al., "From Waste to Resources: Recycling MSW Incineration Ashes in China's Construction Sector," *Journal of the Air & Waste Management Association*, vol. 76, no. 3, pp. 149-168, 2026. [CrossRef] [Google Scholar] [Publisher Link]

[37] Aneeta Mary Joseph et al., "Pre-Treatment and Utilisation of Municipal Solid Waste Incineration Bottom Ashes Towards a Circular Economy," *Construction and Building Materials*, vol. 260, 2020. [CrossRef] [Google Scholar] [Publisher Link]

[38] Haihu Zhang et al., "Cement-Free Binder as a Sustainable Strategy for Maximizing Recycling Municipal Solid Waste Incineration Bottom Ash," *Chemical Engineering Journal*, vol. 536, 2026. [CrossRef] [Google Scholar] [Publisher Link]

[39] Boyu Chen et al., "Advances in using Municipal Solid Waste Incineration (MSWI) Bottom Ash as Precursor for Alkali-Activated Materials: A Critical Review," *Resources, Conservation and Recycling*, vol. 204, pp. 1-21, 2024. [CrossRef] [Google Scholar] [Publisher Link]

[40] R.V. Silva et al., "Use of Municipal Solid Waste Incineration Bottom Ashes in Alkali-Activated Materials, Ceramics and Granular Applications: A Review," *Waste Management*, vol. 68, pp. 207-220, 2017. [CrossRef] [Google Scholar] [Publisher Link]

[41] Sanchit Gupta, and Sandeep Chaudhary, "State of the Art Review on Supplementary Cementitious Materials in India – II: Characteristics of SCMs, Effect on Concrete and Environmental Impact," *Journal of Cleaner Production*, vol. 357, 2022. [CrossRef] [Google Scholar] [Publisher Link]

[42] Sanchit Gupta, and Sandeep Chaudhary, "State of the art Review on Supplementary Cementitious Materials in India – I: An Overview of Legal Perspective, Governing Organizations, and Development Patterns," *Journal of Cleaner Production*, vol. 261, 2020. [CrossRef] [Google Scholar] [Publisher Link]

[43] Ziming Deng et al., "Advantages and Disadvantages of PVA-Fibre-Reinforced Slag- and Fly Ash-Blended Geopolymer Composites: Engineering Properties and Microstructure," *Construction and Building Materials*, vol. 349, 2022. [CrossRef] [Google Scholar] [Publisher Link]

[44] John L. Provis, "Alkali-Activated Materials," *Cement and Concrete Research*, vol. 114, pp. 40-48, 2018. [CrossRef] [Google Scholar] [Publisher Link]

[45] "*Fly Ash Generation at Coal / Lignite based Thermal Power Stations and its Utilization in the Country*," Civil Design Division, Central Electricity Authority, Ministry of Power, New Delhi, Government of India, 2022. [Google Scholar] [Publisher Link]

[46] Boyu Chen et al., "A Review on the Utilization of Municipal Solid Waste Incineration (MSWI) Bottom Ash as a Mineral Resource for Construction Materials," *Journal of Building Engineering*, vol. 71, pp. 1-20, 2023. [CrossRef] [Google Scholar] [Publisher Link]

[47] S. Casanova et al., "Mortars with Alkali-Activated Municipal Solid Waste Incinerator Bottom Ash and Fine Recycled Aggregates," *Journal of Cleaner Production*, vol. 289, 2021. [CrossRef] [Google Scholar] [Publisher Link]

[48] Boyu Chenet al., "Reactivity and Leaching Potential of Municipal Solid Waste Incineration (MSWI) Bottom Ash as Supplementary Cementitious Material and Precursor for Alkali-Activated Materials," *Construction and Building Materials*, vol. 409, pp. 1-21, 2023. [CrossRef] [Google Scholar] [Publisher Link]

[49] X.C. Qiao et al., "Novel Cementitious Materials Produced from Incinerator Bottom Ash," *Resources, Conservation and Recycling*, vol. 52, no. 3, pp. 496-510, 2008. [CrossRef] [Google Scholar] [Publisher Link]

[50] Junjie Zhang et al., "Utilization of Municipal Solid Waste Incinerator Bottom Ash to Prepare Nonautoclaved Aerated Concrete," *Journal of Materials in Civil Engineering*, vol. 38, no. 9, 2026. [CrossRef] [Google Scholar] [Publisher Link]

[51] Jingmei Wang et al., "Comprehensive Assessment of High-Temperature Performance, Economic and Sustainability of MSWI Bottom Ash-Based Alkali-Activated Slag Paste," *Materials*, vol. 19, no. 10, pp. 1-22, 2026. [CrossRef] [Google Scholar] [Publisher Link]

[52] Alireza Bahrami et al., "Toward Sustainable Concrete: Experimental Investigation Using Municipal Solid Waste Incineration Bottom Ash," *Buildings*, vol. 16, no. 7, pp. 1-19, 2026. [CrossRef] [Google Scholar] [Publisher Link]

[53] Zhenlin Li et al., "Harnessing Metallic Aluminum in Incineration Bottom Ash for In-Situ Foamed Lightweight Aggregates: Pore Evolution and Concrete Performance," *Construction and Building Materials*, vol. 538, 2026. [CrossRef] [Google Scholar] [Publisher Link]

[54] Lingzhan Zhou et al., "Critical Threshold Effect and Microscopic Mechanism of Bottom Ash Replacement Ratio in an Alkali-Activated Slag-Bottom Ash System," *Construction and Building Materials*, vol. 509, 2026. [CrossRef] [Google Scholar] [Publisher Link]

[55] Neelam Singh, and Vikas Kumar, "A Review on Sustainable and Effective Utilisation of Municipal Solid Waste Incinerated Ash," *International Journal of Environment and Waste Management*, vol. 39, no. 2, pp. 121-141, 2026. [CrossRef] [Google Scholar] [Publisher Link]

[56] Shin Hau Bong et al., "Ambient Temperature Cured 'Just-Add-Water' Geopolymer for 3D Concrete Printing Applications," *Cement and Concrete Composites*, vol. 121, 2021. [CrossRef] [Google Scholar] [Publisher Link]

[57] Mohammed Ali M. Rihan, and Tareg Abdalla Abdalla, "Advances in One-Part Geopolymer Systems: Fundamentals, Manufacturing, and Comparative Insights with Two-Part Geopolymers," *Waste Management Bulletin*, vol. 4, no. 3, pp. 1-15, 2026. [CrossRef] [Google Scholar] [Publisher Link]

[58] Guruprasad Tumkur Narasimhamurthy, Prashanth Malenahally Hanumanthappa, and Narasimhan Chandrashekhar Mattur, "Development and Characterisation of an Optimum One-part Geopolymer Concrete Mix with High Mechanical Strength," *Progress in Engineering Science*, vol. 3, no. 3, 2026. [CrossRef] [Google Scholar] [Publisher Link]

[59] Naresh Thatikonda et al., "Ambient-Cured One-Part Geopolymer Systems from Industrial by-Products: A Sustainable Chemistry Pathway for Low-Carbon Cementitious Materials," *Sustainable Chemistry and Pharmacy*, vol. 50, 2026. [CrossRef] [Google Scholar] [Publisher Link]

[60] Wei Chen et al., "Time-Dependent Interfacial Pore Evolution and Anisotropic Compressive Response in 3D-Printed One-Part Geopolymer Concrete: Experimental Characterization and Mechanism Modeling," *Materials & Design*, vol. 267, pp. 1-17, 2026. [CrossRef] [Google Scholar] [Publisher Link]

[61] Babatunde Luke Ajayi, Gideon P. A. G. van Zijl, and Adewumi J. Babafemi, "High-Strength Low Paste Volume Ternary-Blended 3D Printed One-part Geopolymer Concrete: Rheology, Hardened Mechanics, and Microstructure," *Journal of Sustainable Cement-Based Materials*, vol. 15, no. 9, pp. 3087-3105, 2026. [CrossRef] [Google Scholar] [Publisher Link]

[62] Daro Sun et al., "Mechanical Properties and Reproducibility of One-Part Ambient-Cured Slag and Fly Ash-Based Geopolymer Concrete," *Buildings*, vol. 16, no. 4, pp. 1-31, 2026. [CrossRef] [Google Scholar] [Publisher Link]

[63] R. Carvalho et al., "Alkali Activation of Bottom Ash from Municipal Solid Waste Incineration: Optimization of NaOH- and Na 2SiO3-based Activators," *Journal of Cleaner Production*, vol. 291, pp. 1-11, 2021. [CrossRef] [Google Scholar] [Publisher Link]

[64] Areej T. Almalkawi, Anagi Balchandra, and Parviz Soroushian, "Potential of Using Industrial Wastes for Production of Geopolymer Binder as Green Construction Materials," *Construction and Building Materials*, vol. 220, pp. 516-524, 2019. [CrossRef] [Google Scholar] [Publisher Link]

[65] Guodong Huang et al., "Effect of Activated Silica on Polymerization Mechanism and Strength Development of MSWI Bottom Ash Alkali-Activated Mortars," *Construction and Building Materials*, vol. 201, pp. 90-99, 2019. [CrossRef] [Google Scholar] [Publisher Link]

[66] Atta Ur Rehman, Sang-Min Lee, and Jung-Hoon Kim, "Use of Municipal Solid Waste Incineration ash in 3D Printable Concrete," *Process Safety and Environmental Protection*, vol. 142, pp. 219-228, 2020. [CrossRef] [Google Scholar] [Publisher Link]

[67] Nikolina Poranek et al., "MSWIBA Formation and Geopolymerisation to Meet the United Nations Sustainable Development Goals (SDGs) and Climate Mitigation," *Buildings*, vol. 12, no. 8, pp. 1-14, 2022. [CrossRef] [Google Scholar] [Publisher Link]

[68] Hengels Castillo et al., "State of the Art of Geopolymers: A Review," *e-Polymers*, vol. 22, no. 1, pp. 108-124, 2022. [CrossRef] [Google Scholar] [Publisher Link]

[69] Yesim Tarhan, Ismail Hakkı Tarhan, and Remzi Sahin, "Comprehensive Review of Binder Matrices in 3D Printing Construction: Rheological Perspectives," *Buildings*, vol. 15, no. 1, pp. 1-50, 2024. [CrossRef] [Google Scholar] [Publisher Link]

[70] Prabhath Ranjan Kumar Soda et al., "Development of 3D Printable Stabilized Earth-Based Construction Materials using Excavated Soil: Evaluation of Fresh and Hardened Properties," *Science of the Total Environment*, vol. 924, 2024. [CrossRef] [Google Scholar] [Publisher Link]

[71] Mona Sando, and Dietmar Stephan, "The Role of Mixing Sequence in Shaping the 3D-Printability of Geopolymers," *Case Studies in Construction Materials*, vol. 22, pp. 1-20, 2025. [CrossRef] [Google Scholar] [Publisher Link]

[72] Nima Aminpour, and Ali Memari, "Analysis of Anisotropic Behavior in 3D Concrete Printing for Mechanical Property Evaluation," *Journal of Building Engineering*, vol. 99, pp. 1-16, 2025. [CrossRef] [Google Scholar] [Publisher Link]

[73] Ibrahim Türkmen et al., "Fresh-State Characteristics of Geopolymer Mortars for 3D Printing: Mix Design, Rheology and Early-Age Performance," *Polymers*, vol. 18, no. 12, pp. 1-29, 2026. [CrossRef] [Google Scholar] [Publisher Link]

[74] Vishakha Sakhare, Mohamed Najar, and Sachin Deshpande, "Printing Performance of 3D-Printed Geopolymer through Pumpability–Extrudability–Buildability Properties – A Review," *Architectural Science Review*, vol. 69, no. 1, pp. 88-112, 2026. [CrossRef] [Google Scholar] [Publisher Link]

[75] Shin Hau Bong et al., "Efficiency of Different Superplasticizers and Retarders on Properties of 'One-Part' Fly Ash-Slag Blended Geopolymers with Different Activators," *Materials*, vol. 12, no. 20, pp. 1-17, 2019. [CrossRef] [Google Scholar] [Publisher Link]

[76] Shravan Muthukrishnan, Sayanthan Ramakrishnan, and Jay Sanjayan, "Effect of Alkali Reactions on the Rheology of One-Part 3D Printable Geopolymer Concrete," *Cement and Concrete Composites*, vol. 116, pp. 1-49, 2021. [CrossRef] [Google Scholar] [Publisher Link]

[77] Biranchi Panda et al., "Synthesis and Characterization of One-Part Geopolymers for Extrusion based 3D Concrete Printing," *Journal of Cleaner Production*, vol. 220, pp. 610-619, 2019. [CrossRef] [Google Scholar] [Publisher Link]

[78] Joseph Davidovits, *Geopolymer Chemistry and Applications*, Geopolymer Institute, pp. 1-680, 2008. [Google Scholar] [Publisher Link]

[79] Nicolas Roussel, "Rheological Requirements for Printable Concretes," *Cement and Concrete Research*, vol. 112, pp. 76-85, 2018. [CrossRef] [Google Scholar] [Publisher Link]

[80] Yi Wei Daniel Tay, Ye Qian, and Ming Jen Tan, "Printability Region for 3D Concrete Printing using Slump and Slump Flow Test," *Composites Part B: Engineering*, vol. 174, 2019. [CrossRef] [Google Scholar] [Publisher Link]

[81] Yi Wei Daniel Tay, "*Large Scale 3D Concrete Printing: Process and Materials Properties*," Thesis, Nanyang Technological University, pp. 1-205, 2020. [CrossRef] [Google Scholar] [Publisher Link]

[82] Suvash Chandra Paul et al., "Fresh and Hardened Properties of 3D Printable Cementitious Materials for Building and Construction," *Archives of Civil and Mechanical Engineering*, vol. 18, pp. 311-319, 2018. [CrossRef] [Google Scholar] [Publisher Link]

[83] Eugene Cook Bingham, *Fluidity and Plasticity*, McGraw-Hill Book Company, pp. 1-440, 1922. [Google Scholar] [Publisher Link]

[84] Mehdi Chougan et al., "The Influence of Nano-Additives in Strengthening Mechanical Performance of 3D Printed Multi-Binder Geopolymer Composites," *Construction and Building Materials*, vol. 250, pp. 1-13, 2020. [CrossRef] [Google Scholar] [Publisher Link]

[85] Yu Zhang et al., "Fresh Properties of a Novel 3D Printing Concrete Ink," *Construction and Building Materials*, vol. 174, pp. 263-271, 2018. [CrossRef] [Google Scholar] [Publisher Link]

[86] Olafur H. Wallevik et al., "Avoiding Inaccurate Interpretations of Rheological Measurements for Cement-Based Materials," *Cement and Concrete Research*, vol. 78, pp. 100-109, 2015. [CrossRef] [Google Scholar] [Publisher Link]

[87] Stefan Chaves Figueiredo et al., "An Approach to Develop Printable Strain Hardening Cementitious Composites," *Materials & Design*, vol. 169, pp. 1-17, 2019. [CrossRef] [Google Scholar] [Publisher Link]

[88] Mien V. Tran, Tran H. Vu, and Thi Hai Yen Nguyen, "Simplified Assessment for One-Part 3D-Printable Geopolymer Concrete based on Slump and Slump Flow Measurements," *Case Studies in Construction Materials*, vol. 18, pp. 1-12, 2023. [CrossRef] [Google Scholar] [Publisher Link]

[89] Fazlul Hoque Tushar et al., "Factors Affecting Flowability and Rheological Behavior of 3D Printed Concrete: A Comprehensive Review," *Construction and Building Materials*, vol. 508, 2026. [CrossRef] [Google Scholar] [Publisher Link]

[90] M. Papachristoforou, V. Mitsopoulos, and M. Stefanidou, "Evaluation of Workability Parameters in 3D Printing Concrete," *Procedia Structural Integrity*, vol. 10, pp. 155-162, 2018. [CrossRef] [Google Scholar] [Publisher Link]

[91] Mona Sando, and Dietmar Stephan, "The Development of a Fly Ash-BASED Geopolymer for Extrusion-based 3D Printing, along with a Printability Prediction Method," *Case Studies in Construction Materials*, vol. 21, pp. 1-25, 2024. [CrossRef] [Google Scholar] [Publisher Link]

[92] Shuai Zou et al., "On Rheology of Mortar with Recycled Fine Aggregate for 3D Printing," *Construction and Building Materials*, vol. 311, 2021. [CrossRef] [Google Scholar] [Publisher Link]

[93] Astha Sharma et al., "Factors Affecting the Rheology of Cement-Based Composites: A Review," *Journal of the American Ceramic Society*, vol. 108, no. 6, pp. 1-33, 2025. [CrossRef] [Google Scholar] [Publisher Link]

[94] Shaodan Hou et al., "Rheology of Fiber-Reinforced Mortar for 3D Printing Construction: Effect of Recycled Hybrid Powder and Polyethylene Fiber," *Construction and Building Materials*, vol. 447, 2024. [CrossRef] [Google Scholar] [Publisher Link]

[95] Timothy Wangler et al., "Digital Concrete: Opportunities and Challenges," *RILEM Technical Letters*, vol. 1, no. 1, pp. 67-75, 2017. [CrossRef] [Google Scholar] [Publisher Link]

[96] Dimitri Feys et al., "Extension of the Reiner–Riwlin Equation to Determine Modified Bingham Parameters Measured in Coaxial Cylinders Rheometers," *Materials and Structures*, vol. 46, no. 1, pp. 289-311, 2013. [CrossRef] [Google Scholar] [Publisher Link]

[97] Qi Deng et al., "Rheological Properties of Mortar with Recycled Fine Aggregate: From the Perspective of Particle Packing," *Construction and Building Materials*, vol. 465, 2025. [CrossRef] [Google Scholar] [Publisher Link]

[98] Kala Kondepudi et al., "Study of Particle Packing and Paste Rheology in Alkali Activated Mixtures to Meet the Rheology Demands of 3D Concrete Printing," *Cement and Concrete Composites*, vol. 131, pp. 1-14, 2022. [CrossRef] [Google Scholar] [Publisher Link]

[99] Pei Tang et al., "Investigation of Cementitious Properties of Different Constituents in Municipal Solid Waste Incineration Bottom Ash as Supplementary Cementitious Materials," *Journal of Cleaner Production*, vol. 258, 2020. [CrossRef] [Google Scholar] [Publisher Link]

[100] Weiping Zhu et al., "Strategic Utilization of Municipal Solid Waste Incineration Bottom Ash for the Synthesis of Lightweight Aerated Alkali-Activated Materials," *Journal of Cleaner Production*, vol. 235, pp. 603-612, 2019. [CrossRef] [Google Scholar] [Publisher Link]

[101] Guowei Ma et al., "Effect of Steel Slag on 3D Concrete Printing of Geopolymer with Quaternary Binders," *Ceramics International*, vol. 48, no. 18, pp. 26233-26247, 2022. [CrossRef] [Google Scholar] [Publisher Link]

[102] Huseyin Ilcan et al., "Rheological Properties and Compressive Strength of Construction and Demolition Waste-Based Geopolymer Mortars for 3D-Printing," *Construction and Building Materials*, vol. 328, 2022. [CrossRef] [Google Scholar] [Publisher Link]

[103] Nazim Cagatay Demiral et al., "Mechanical Anisotropy Evaluation and Bonding Properties of 3D-Printable Construction and Demolition Waste-based Geopolymer Mortars," *Cement and Concrete Composites*, vol. 134, 2022. [CrossRef] [Google Scholar] [Publisher Link]

[104] Oğuzhan Şahin et al., "Construction and Demolition Waste-Based Geopolymers Suited for Use in 3-Dimensional Additive Manufacturing," *Cement and Concrete Composites*, vol. 121, 2021. [CrossRef] [Google Scholar] [Publisher Link]

[105] T.T. Le et al., "Hardened Properties of High-Performance Printing Concrete," *Cement and Concrete Research*, vol. 42, no. 3, pp. 558-566, 2012. [CrossRef] [Google Scholar] [Publisher Link]

[106] R.J.M. Wolfs, F.P. Bos, and T.A.M. Salet, "Hardened Properties of 3D Printed Concrete: The Influence of Process Parameters on Interlayer Adhesion," *Cement and Concrete Research*, vol. 119, pp. 132-140, 2019. [CrossRef] [Google Scholar] [Publisher Link]

[107] Marchant van den Heever et al., "Evaluating the Effects of Porosity on the Mechanical Properties of Extrusion-based 3D Printed Concrete," *Cement and Concrete Research*, vol. 153, 2022. [CrossRef] [Google Scholar] [Publisher Link]

[108] Mohammad R. Irshidat, Nasser Al-Nuaimi, and Mohamed Rabie, "Sustainable Alkali-Activated Binders with Municipal Solid Waste Incineration Ashes as Sand or Fly Ash Replacement," *Journal of Material Cycles and Waste Management*, vol. 24, no. 3, pp. 992-1008, 2022. [CrossRef] [Google Scholar] [Publisher Link]

[109] Guowei Ma et al., "Mechanical Characterization of 3D Printed Anisotropic Cementitious Material by the Electromechanical Transducer," *Smart Materials and Structures*, vol. 27, no. 7, 2018. [CrossRef] [Google Scholar] [Publisher Link]

[110] Biranchi Panda et al., "Additive Manufacturing of Geopolymer for Sustainable Built Environment," *Journal of Cleaner Production*, vol. 167, pp. 281-288, 2017. [CrossRef] [Google Scholar] [Publisher Link]

[111] Àlex Maldonado-Alameda et al., "Municipal Solid Waste Incineration Bottom Ash as Sole Precursor in the Alkali-Activated Binder Formulation," *Applied Sciences*, vol. 10, no. 12, pp. 1-15, 2020. [CrossRef] [Google Scholar] [Publisher Link]

[112] Nuno Cristelo et al., "Recycling Municipal Solid Waste Incineration Slag and Fly Ash as Precursors in Low-Range Alkaline Cements," *Waste Management*, vol. 104, pp. 60-73, 2020. [CrossRef] [Google Scholar] [Publisher Link]

[113] X. Gao et al., "Characterization and Application of Municipal Solid Waste Incineration (MSWI) Bottom Ash and Waste Granite Powder in Alkali Activated Slag," *Journal of Cleaner Production*, vol. 164, pp. 410-419, 2017. [CrossRef] [Google Scholar] [Publisher Link]

[114] Isabella Lancellotti et al., "Alkali Activation Processes for Incinerator Residues Management," *Waste Management*, vol. 33, no. 8, pp. 1740-1749, 2013. [CrossRef] [Google Scholar] [Publisher Link]

[115] Shantanu Bhattacherjee et al., "Sustainable Materials for 3D Concrete Printing," *Cement and Concrete Composites*, vol. 122, 2021. [CrossRef] [Google Scholar] [Publisher Link]

[116] Keun-Hyeok Yang, Jin-Kyu Song, and Keum-Il Song, "Assessment of CO2 Reduction of Alkali-Activated Concrete," *Journal of Cleaner Production*, vol. 39, pp. 265-272, 2013. [CrossRef] [Google Scholar] [Publisher Link]

[117] Evan Jamieson, Benjamin McLellan, and Arie van Riessen, "Comparison of Embodied Energies of Ordinary Portland Cement with Bayer-Derived Geopolymer Products," *Journal of Cleaner Production*, vol. 99, pp. 112-118, 2015. [CrossRef] [Google Scholar] [Publisher Link]

[118] G. Habert, J.B. d'Espinose de Lacaillerie, and N. Roussel, "An Environmental Evaluation of Geopolymer based Concrete Production: Reviewing Current Research Trends," *Journal of Cleaner Production*, vol. 19, no. 11, pp. 1229-1238, 2011. [CrossRef] [Google Scholar] [Publisher Link]

[119] IEA Bioenergy, "*Municipal Solid Waste and its Role in Sustainability*," International Energy Agency, pp. 1-7, 2003. [Google Scholar] [Publisher Link]

[120] Rahul Sharma, and Rizwan A. Khan, "Sustainable use of Copper slag in Self Compacting Concrete Containing Supplementary Cementitious Materials," *Journal of Cleaner Production*, vol. 151, pp. 179-192, 2017. [CrossRef] [Google Scholar] [Publisher Link]

[121] Matthias Fawer, Martin Concannon, and Wolfram Rieber, "Life Cycle Inventories for the Production of Sodium Silicates," *The International Journal of Life Cycle Assessment*, vol. 4, no. 4, pp. 207-212, 1999. [CrossRef] [Google Scholar] [Publisher Link]

[122] Xiaoyan Huang, Ravi Ranade, and Victor C. Li, "Feasibility Study of Developing Green ECC Using Iron Ore Tailings Powder as Cement Replacement," *Journal of Materials in Civil Engineering*, vol. 25, no. 7, pp. 923-931, 2013. [CrossRef] [Google Scholar] [Publisher Link]

[123] En-Hua Yang, Yingzi Yang, and Victor C. Li, "Use of High Volumes of Fly Ash to Improve ECC Mechanical Properties and Material Greenness," *Materials Journal*, vol. 104, no. 6, pp. 620-628, 2007. [CrossRef] [Google Scholar] [Publisher Link]

[124] Peter W. Rein, "The Carbon Footprint of Sugar," *Sugar Industry*, vol. 135, no. 7, 427-434, 2010. [CrossRef] [Google Scholar] [Publisher Link]

[125] Xiaoyan Wei et al., "Mechanical and Environmental Performance of Chemical Pretreated Incineration Bottom Ash as a Supplementary Cementitious Material," *Materials*, vol. 19, no. 4, pp. 1-29, 2026. [CrossRef] [Google Scholar] [Publisher Link]

[126] Maria Júlia Bassan de Moraes et al., "Alkali Activated Materials Applied in 3D Printing Construction: A Review," *Heliyon*, vol. 10, no. 5, pp. 1-30, 2024. [CrossRef] [Google Scholar] [Publisher Link]

[127] Qian Yu et al., "Investigation of the Rheological and Mechanical Properties of 3D Printed Eco-Friendly Concrete with Steel Slag," *Journal of Building Engineering*, vol. 72, 2023. [CrossRef] [Google Scholar] [Publisher Link]

[128] A. Perrot, D. Rangeard, and A. Pierre, "Structural Built-up of Cement-based Materials used for 3D-Printing Extrusion Techniques," *Materials and Structures*, vol. 49, pp. 1213-1220, 2016. [CrossRef] [Google Scholar] [Publisher Link]

[129] A. Perrot et al., "Prediction of Lateral form Pressure Exerted by Concrete at Low Casting Rates," *Materials and Structures*, vol. 48, no. 7, pp. 2315-2322, 2015. [CrossRef] [Google Scholar] [Publisher Link]